

Excitation and radiative decay of the 184.9 Nm Hg resonance line in low-pressure mercury noble-gas discharges

Citation for published version (APA):

Post, H. A. (1985). *Excitation and radiative decay of the 184.9 Nm Hg resonance line in low-pressure mercury noble-gas discharges*. [Phd Thesis 1 (Research TU/e / Graduation TU/e), Applied Physics and Science Education]. Technische Hogeschool Eindhoven. <https://doi.org/10.6100/IR214998>

DOI:

[10.6100/IR214998](https://doi.org/10.6100/IR214998)

Document status and date:

Published: 01/01/1985

Document Version:

Publisher's PDF, also known as Version of Record (includes final page, issue and volume numbers)

Please check the document version of this publication:

- A submitted manuscript is the version of the article upon submission and before peer-review. There can be important differences between the submitted version and the official published version of record. People interested in the research are advised to contact the author for the final version of the publication, or visit the DOI to the publisher's website.
- The final author version and the galley proof are versions of the publication after peer review.
- The final published version features the final layout of the paper including the volume, issue and page numbers.

[Link to publication](#)

General rights

Copyright and moral rights for the publications made accessible in the public portal are retained by the authors and/or other copyright owners and it is a condition of accessing publications that users recognise and abide by the legal requirements associated with these rights.

- Users may download and print one copy of any publication from the public portal for the purpose of private study or research.
- You may not further distribute the material or use it for any profit-making activity or commercial gain
- You may freely distribute the URL identifying the publication in the public portal.

If the publication is distributed under the terms of Article 25fa of the Dutch Copyright Act, indicated by the "Taverne" license above, please follow below link for the End User Agreement:

www.tue.nl/taverne

Take down policy

If you believe that this document breaches copyright please contact us at:

openaccess@tue.nl

providing details and we will investigate your claim.

**EXCITATION AND RADIATIVE DECAY OF THE
184.9 nm Hg RESONANCE LINE IN
LOW-PRESSURE MERCURY NOBLE-GAS DISCHARGES**

PROEFSCHRIFT

ter verkrijging van de graad van doctor in de
technische wetenschappen aan de Technische
Hogeschool Eindhoven, op gezag van de rector
magnificus, prof. dr. F.N. Hooge, voor een
commissie aangewezen door het college van
dekanen in het openbaar te verdedigen op
vrijdag 18 oktober 1985 te 14.00 uur

door

HENDRIK ARIËN POST

geboren te Nijmegen

Dit proefschrift is goedgekeurd door de promotoren:

Prof. Dr. Ir. H.L. Hagedoorn

Prof. Dr. Ir. D.C. Schram

Aan mijn ouders

Aan Ems

Ariënne
Pauline
Annemarie

CONTENTS

I. Introduction	1
I.1. Hg 6^1P_1 excitation cross sections	2
I.2. Radiative transport	3
II. Experimental	7
II.1. Dye laser absorption measurements	7
II.2. Laser-induced fluorescence measurements	9
II.3. Emission measurements	11
III. The absolute Hg 6^1P_1 direct electron impact excitation cross section determined in a low-pressure Hg discharge	13
III.1. Principle of the method	13
III.2. Experimental results and analysis	15
III.2.1. Axial inhomogeneity	15
III.2.2. Density measurements	16
III.2.3. Radial profiles	18
III.2.4. Decay measurements	19
III.2.5. Experimental conditions	21
III.2.6. Optical excitation functions	21
III.2.7. Absolute cross section scale	22
III.3. Comparison with literature	25
Appendix III	27
IV. Radiative transport at the 184.9 nm Hg resonance line. Theory	31
IV.1. General formulation	31
IV.1.1. Transport equation	31
IV.1.2. Frequency redistribution function	33
IV.1.3. Radiative decay rate	34
IV.2. Application to an infinite cylinder	40
IV.2.1. Spectral line shape	40
IV.2.2. Effective escape function	42
IV.2.3. Integrand of expression for β	43
IV.2.4. Radial profile $f(\rho, x)$	45
IV.3. Discussion	46
Appendix IV.A	49
Appendix IV.B	50
Appendix IV.C	53

V. Radiative transport at the 184.9 nm Hg resonance line.	
Experimental results and analysis	57
V.1. Dye laser absorption measurements	58
V.1.1. Zero perturber gas pressure	58
V.1.1.1. Decay measurements	58
V.1.1.2. Radiative decay rate	59
V.1.2. Mercury noble-gas mixtures	63
V.2. Laser-induced fluorescence measurements	67
V.3. Comparison with theory	70
VI. Concluding remarks	75
Summary	77
Samenvatting	80
Dankwoord	83
Curriculum vitae	84

The investigations described in this thesis have been published in, or have been submitted to, the following journals:

Chapter III: H.A. Post, *J. Phys.* **B17**, 3193 (1984).

Chapter IV: H.A. Post, submitted to *Phys. Rev. A*.

Chapter V : H.A. Post, P. van de Weijer and R.M.M. Cremers, submitted to *Phys. Rev. A*.

A preliminary account of the work described in chapter IV and part of chapter V is given in: H.A. Post, Abstracts 7th ESCAMPIG, Bari, Europhys. Conf. Abstracts 8E, 150 (1984)

The subject of this thesis is a quantitative study of the main processes responsible for the UV output at the 184.9 nm line (see fig. 1.1) of low-pressure mercury noble-gas discharges. These processes are

- i. excitation of the 6^1P_1 level by electron impact from the 6^1S_0 ground state as well as from the nearby 3^3P states.
- ii. radiative decay of the 6^1P_1 population under the influence of strong radiation trapping at the 184.9 nm resonance line. Due to this process the escape rate of the resonance photons from the volume can be several orders of magnitude lower than the natural decay rate of the dipole transition.

For both processes no sufficiently reliable quantitative data nor theoretical expressions to calculate them from were available in the literature. However, such data are essential if we want to calculate the radiated power at the 184.9 nm line from the microscopic discharge parameters, as is frequently done in model calculations. We studied these processes quantitatively from both the experimental and the theoretical point of view.

In the following we will first discuss the processes under i. (chapter III), and secondly the processes related to ii. (chapters IV, V).

1.1. Hg 6^1P_1 excitation cross sections

Reliable cross sections for the electron impact excitation of the Hg 6^1P_1 level were not available in the literature at the time this study was initiated. The reported cross section values for direct excitation of the 6^1P_1 state show much disagreement, both experimental (Arn 35, Jon 62) and theoretical (Pen 32, Yav 47, McC 68, Sav 70). Values for excitation of the 6^1P_1 state from the nearby 6^3P states are unknown. In chapter III the direct excitation of the 6^1P_1 state is considered. An estimate of the indirect excitation cross sections is given in appendix III.

Absolute values for the optical excitation function of the line λ , $\alpha_\lambda(E_0)$, for excitation by electron impact on ground state atoms are difficult to obtain for a strong resonance line (Moi 68). In most cases only the relative functions are measured. For the 184.9 nm line the relative function has been measured in perpendicular beam experiments (Ott 74, McL 82). From our experiments an absolute scale is obtained. The experiments were performed in a low-pressure Hg discharge ($p_{\text{Hg}} < 1 \text{ Pa}$) in the regime where electron impact excitation from the ground state is dominant (Kag 67, Wei 82) and depopulation of the levels consists mainly of radiative decay.

The radiative decay rate at a line is then equal to the optical excitation

rate. For the 184.9 nm line we obtained the rate from measurements of the 6^1P_1 density in the steady state and its decay time in the afterglow of the discharge with a dye laser absorption method. This avoids the problems attached to the measurement of absolute 184.9 nm radiative power, and at the same time provides information on the radial density profile of the 6^1P_1 state. The absolute scale of $\sigma_{184.9}(E_e)$ is then obtained by comparing the radiative decay rate of the 184.9 nm line with the rates of a number of optically thin lines with known absolute $\sigma_\lambda(E_e)$ (Jon 62, And 67). The latter rates were derived from the measured absolute radiances at the lines. In the analysis we use the experimental fact that the electron energy distribution is Maxwellian in this discharge regime (Lan 24, Vor 64, Ray 68, Mil 78).

The details of the experimental set-up are described in chapter II. In section III.1. the principle of the method is outlined first. The experimental results are presented in section III.2. and the absolute cross section scale is obtained from the analysis of the data. Section III.3. contains a comparison of the absolute cross section as measured here with the data reported in the literature.

1.2. Radiative transport

The transport of resonance radiation has been treated by Holstein (Hol 47, 51), Biberman (Bib 47, 49) and others (Pay 70, Tri 76a) on the assumption known as complete redistribution in frequency. This assumption implies that the line profile of the radiation emitted from a given volume element is proportional to the absorption line profile of the medium. The effects of correlations existing between the absorbed and emitted photon frequencies in the individual absorption-reemission events are then supposed to be negligible. This is justified in the limit of many decorrelating collisions (elastic collision rate γ_c) within a natural lifetime $\tau_0 = 1/\gamma$, i.e. when $\gamma_c/\gamma \gg 1$ (Hol 47, 51). It has been shown by Monte Carlo calculations (Klo 72) as well as analytically (Pay 74, Tri 76b) that, if in contrast $\gamma_c/\gamma \ll 1$, the radiative decay after a few natural lifetimes is also predicted well with this assumption, provided that the optical thickness is large and the wings of the Voigt absorption line profile are optically thin and contribute relatively little to the total emission. This is equivalent to the limiting case of a pure Doppler broadened absorption line profile (see chapter IV). With complete redistribution in frequency the radiative transfer problem depends only on the optical thickness at the line centre and on the absorption line profile. Exact and approximate solutions have been given by many authors (Hol 47, 51; Bib 47, 49; Pay 70, Tri 76a, Pay 74, Klo 72).

However, sizeable deviations from the complete redistribution results occur if the wings of the Voigt absorption line profile are important in the low collision rate ($\gamma_c/\gamma \ll 1$), large optical thickness regime (Pay 74). An expression for the radiative decay rate in this case also depends explicitly on the ratio γ_c/γ . It has only been given for the rate of the early time escape following pulsed pencil-like excitation along the axis of a cylinder in combination with side-on observation of a slab region around this axis (Pay 74). However, in many laboratory experimental situations an expression for the radiative decay rate in the fundamental mode, i.e. 'at late times', would be more useful. Such an expression is lacking up till now.

For the discharge conditions of fluorescent lamp operation the assumption of complete redistribution in frequency fails for the radiative transport at the 184.9 nm line ($6^1P_1-6^1S_0$); see chapters IV, V. In section IV.1. a partial redistribution theory is described for the fundamental mode radiative decay rate β , which is an extension of the work of Payne *et al.* (Pay 74). The analytical expression for β , obtained for a resonance line with hyperfine structure, is valid for large optical thickness and a vast range of γ_c/γ values. A condition for the existence of a fundamental mode is discussed and is shown to be largely satisfied in our experiments. In section IV.2. the theory is applied to the case of an infinite cylinder and several results, as e.g. the shape of the emission line profile, are considered in more detail. Furthermore, an approximation is discussed which considerably simplifies the calculation of β at the expense of only a small error. In section V we report on measurements of the fundamental mode radiative decay rate of the Hg 6^1P_1 population under conditions of low collision rate and large optical thickness of the 184.9 nm resonance line. In these measurements the decay rate of the 6^1P_1 population was measured in the afterglow of a low-pressure mercury noble-gas discharge using a dye laser absorption technique. We report also on measurements of the radiative decay rate performed by a colleague, Dr. P. van de Weijer. These measurements were made using a different experimental method also employing a low-pressure mercury noble-gas discharge. In this method the decay was measured of the laser-induced fluorescence (LIF) at the 189.4 nm line, created by pulsed optical pumping. The results of this LIF method are used extensively in this thesis for a comparison with the theory of chapter IV. Therefore it seems reasonable to include a brief description of the experimental method. The combined measured data extend over a wide range of experimental conditions.

The experimental arrangements are described in chapter II. In sections V.1. and V.2. an analysis is given of the data and the resulting radiative decay rates are compared with calculated values from theory using the complete

redistribution assumption. In section V.3. the experimental decay rates are compared with calculated ones using the partial redistribution theory described in chapter IV.

Chapter VI contains some concluding remarks.

REFERENCES

- And 67 R. J. Anderson, E. T. P. Lee and C. C. Lin, *Phys. Rev.* **157**, 31 (1967).
Arn 35 F. L. Arnot and G. O. Baines, *Proc. Roy. Soc.* **A151**, 256 (1935).
Bar 60 B. T. Barnes, *J. Appl. Phys.* **31**, 852 (1960).
Bib 47 L. M. Biberman, *Zh. Eksp. Teor. Fiz.* **17**, 416 (1947).
Bib 49 L. M. Biberman, *Zh. Eksp. Teor. Fiz.* **17**, 584 (1949).
Hol 47 T. Holstein, *Phys. Rev.* **72**, 1212 (1947).
Hol 51 T. Holstein, *Phys. Rev.* **83**, 1159 (1951).
Jon 62 H. M. Jongerius, *Philips Res. Rep. Suppl.* **2**, (1962).
Kag 67 Yu. M. Kagan and B. Kasmaliev, *Opt. Spectr.* **22**, 293 (1967).
Klo 72 C. E. Klots and V. E. Anderson, *J. Chem. Phys.* **56**, 120 (1972).
Koe 63 M. Koedam, A. A. Kruithof and J. Riemens, *Physica* **29**, 565 (1963).
Lan 24 I. Langmuir and H. Mott-Smith, *Gen. Electr. Rev.* **27**, 616 (1924).
McC 68 J. C. McConnell and B. L. Moiseiwitsch, *J. Phys. B. (Proc. Phys. Soc.)* **1**, 406 (1968).
McL 82 C. W. McLucas, H. J. E. Wehr, W. R. MacGillivray and M. C. Standage, *J. Phys.* **B15**, 1883 (1982).
Mil 78 V. M. Milenin and N. A. Timofeev, *Sov. Phys. Tech. Phys.* **23**, 1048 (1978).
Moi 68 B. L. Moiseiwitsch and S. J. Smith, *Rev. Mod. Phys.* **40**, 238 (1968).
Moo 58 C. E. Moore, 'Atomic Energy Levels', Vol. 3, NBS Circ. 467, Washington DC (1958).
Ott 74 T. W. Ottley, D. R. Denne and H. Kleinpoppen, *J. Phys.* **B7**, L179 (1974).
Pay 70 M. G. Payne and J. D. Cook, *Phys. Rev.* **A2**, 1238 (1970).
Pay 74 M. G. Payne, J. E. Talmage, G. S. Hurst and E. B. Wagner, *Phys. Rev.* **A9**, 1050 (1974).
Pen 32 W. G. Penney, *Phys. Rev.* **39**, 467 (1932).
Ray 68 S. W. Rayment and N. D. Twiddy, *Proc. Roy. Soc.* **A304**, 87 (1968).
Sav 70 V. N. Savchenko, *Opt. Spectr.* **30**, 6 (1970).
Tri 76a C. van Trigt, *Phys. Rev.* **A13**, 726 (1976).
Tri 76b C. van Trigt, *Phys. Rev.* **A13**, 734 (1976).
Vor 64 N. A. Vorob'eva, Yu. M. Kagan, R. J. Lyagushchenko and V. M. Milenin, *Sov. Phys. Tech. Phys.* **9**, 114 (1964).
Wei 82 P. van de Weijer and R. M. M. Cremers, *J. Appl. Phys.* **53**, 1401 (1982).
Yav 47 B. M. Yavorskii, *Zh. Eksp. Teor. Fiz.* **17**, 315 (1947).

II. Experimental

In this section we will describe the experimental arrangements. These were used for the measurements of the Hg 6^1P_1 density (section II.1.), and its radiative decay rate β under conditions of strong radiation trapping at the 184.9 nm resonance line (sections II.1., II.2.). Furthermore we measured the absolute radiances of emission lines in a direction normal to the discharge tube (section II.3.).

In all experiments the mercury consisted of a natural mixture of isotopes.

II.1. Dye laser absorption measurements

The density in the 6^1P_1 level was determined by measuring the absorption at hyperfine components of the 579.1 nm line ($6^1P_1 - 6^1D_2$), see fig. 1-1. Beer's law was used to determine the density from the measured absorption. The radiative decay rate of the 184.9 nm resonance line was derived by measuring the decay of the 6^1P_1 density in the afterglow of the discharge.

The relation between the density n in the lower level of the absorption line transition and the decrease of the laser beam spectral intensity $I_\nu(z)$ along the absorption pathlength l in the z direction is given by Beer's law (Mit 71):

$$\begin{aligned} \ln \frac{I_\nu(l)}{I_\nu(0)} &= -k(\nu)l \\ &= -c_0 n f l \mathcal{L}(\nu - \nu_0). \end{aligned} \quad (2.1)$$

Here it is assumed that the density in the upper level of the transition is much smaller than that in the lower one. Further $k(\nu)$ is the absorption coefficient, ν is the frequency, ν_0 is the frequency at the line centre, f is the oscillator strength, $\mathcal{L}(\nu - \nu_0)$ is the normalized absorption line profile and c_0 is a numerical constant equal to $c_0 = \frac{1}{12.1 \pi}$.

The Pyrex cylindrical discharge tubes are U-shaped (see fig. 2-1) in order to allow the measurement of the axially averaged 6^1P_1 densities at the selected radial position. The values of the inner radius R in the central straight part of the tube were $R = 6.2, 9.7, 12.5, 17.7$ mm for zero noble gas pressure and $R = 17.7$ mm for Ar pressures of 33 and 67 Pa. The temperature of the tube wall in this part of the tube, T_w , and of an appendix, T_{Hg} , could be controlled independently by water from two thermostats. The appendix A was located in the middle of the tube and served as the coldest

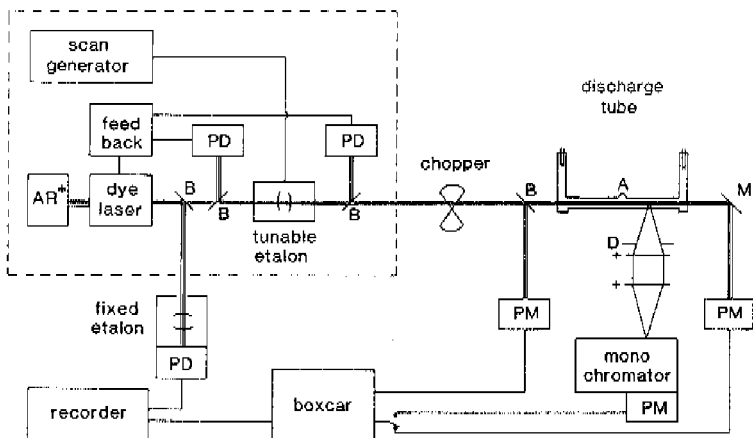


Fig. 2-1. Schematic diagram of the experimental set-up used for the dye laser absorption measurements as well as for the absolute emission measurements. The outer tubes surrounding the discharge tube and the appendix A (see text) have not been shown for reasons of simplicity. PD = photodetector, PM = photomultiplier, B = beam splitter, D = diaphragm, M = mirror.

spot which determines the mercury vapour pressure. Its temperature T_{Hg} is quoted throughout the paper and was always 1°C lower than T_w . The bends as well as both side legs of the U-shaped tubes were slightly heated to prevent their surface from becoming the coldest spot. Of the discharge tubes used for the measurement of the radiative decay rates (chapter V) the three legs of the U-shape were 0.07, 0.50, 0.07 m long, respectively.

The tube used to determine the absolute cross section (chapter III) differed from the other ones in some respects:

- i. the three legs of the U-shape measured 0.40, 0.30, 0.40 m, and had the same inner radius $R = 12.5$ mm.
- ii. the two outer legs were thermostated in the same way as the central one.
- iii. a less good axial homogeneity of the central part of the tube due to the presence of two wider sections (radius 20 mm) at the bends with length 0.04 m (this was 0.02 m in the other tubes).

The inner surface of the discharge tubes was coated with a thin layer of Y_2O_3 . This provided a faster stabilization in a new experimental condition than obtained with the uncoated Pyrex tube wall, due to the lower adsorption energy of Hg on Y_2O_3 than on Pyrex. The mercury vapour pressure ranged from 0.17 to 12 Pa. With zero noble gas pressure the discharge current range was 1.5 – 150 mA, with non-zero Ar pressure it was 5 – 1000 mA.

The discharge was operated quasi-DC by means of an electronic commutator, the current waveform being a symmetrical block with a frequency of 175 Hz. Thanks to these precautions the influence of electrophoretic and cataphoretic effects upon the axial number densities is negligible under our conditions (Ken 38). After the initiation of the afterglow the discharge voltage dropped within $0.2 \mu\text{s}$ to $\sim 1\%$ of its steady state value.

The experimental arrangement used for the dye laser absorption measurements is illustrated in fig. 2.1. The single-mode Rhodamine 6G dye laser (Spectra Physics 580), pumped by an Ar ion laser (Spectra Physics 170), was stabilized on an external tunable etalon (frequency drift $< 100 \text{ MHz/min}$). The etalon with free spectral range (FSR) = 7.5 GHz and finesse ~ 75 was also used as a narrow-band filter. This was done to suppress spurious adjacent cavity modes with a mode distance of 500 MHz . The dye laser output frequency spectrum was monitored by a fixed etalon of known FSR (1500 MHz) to calibrate the wavelength scale of the absorption line shape measurements. The laser beam traverses the discharge tube, the transmitted and reference beam intensities being detected by two photomultipliers. The laser beam was chopped with duty cycle 1:12, synchronously with the presence of the afterglow. The RC time constant of the detection system was $\sim 0.2 \mu\text{s}$. A two-channel PAR 162 boxcar integrator was used to measure the log-ratio of these signals in the afterglow as well as in the steady state of the discharge.

II.2. Laser-induced fluorescence measurements

The discharge tubes were irradiated side-on with a dye laser pulse at 365.5 nm , thus exciting mercury atoms from the metastable 6^3P_2 level to the 6^3D_2 level (see fig. 2.2). The 6^3D_2 level decays radiatively with a time constant of 9 ns (Bor 79) to the 6^3P_2 , 6^3P_1 and 6^1P_1 levels. At sufficiently low discharge currents the fluorescence at the 184.9 nm line resulting from this temporary overpopulation of the 6^1P_1 level provides the radiative decay rate of the 184.9 nm resonance line (see fig. 2.3).

The tubes containing the mercury (noble gas) discharges are centered in wider outer tubes. Water, flowing between inner and outer tube, is used to control the temperature of the inner tube. As water is not transparent to 184.9 nm radiation, two separate outer tubes are used for each discharge tube. In this way a small part of the discharge tube is not surrounded by the water bath, thus enabling us to detect the 184.9 nm fluorescence. However, a coldest spot would be introduced in this way for water temperatures higher than ambient. In order to prevent this, the 'naked' part of the discharge tube

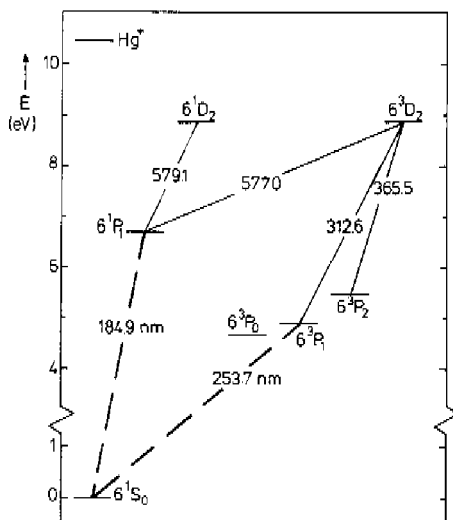


Fig. 2-2. Partial energy level scheme of Hg^+ , showing the atomic transitions used in the dye laser absorption and the laser-induced fluorescence experiments. Transitions indicated with solid (dashed) lines are optically thin (thick) for our experimental conditions.

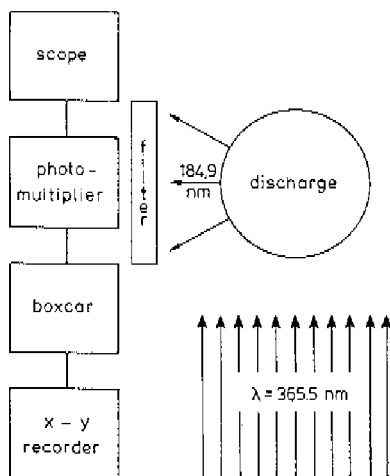


Fig. 2-3. Schematic diagram of the experimental set-up used for the laser-induced fluorescence measurements.

was surrounded by heating wire. For every data point the mercury vapour density n_{Hg} was checked by the measurement of the radiative decay rate of the 6^3P_1 level, which is known as a function of n_{Hg} in our conditions (Wei 85). These 253.7 nm fluorescence measurements could be performed with the same pumping wavelength, since the 312.6 nm line, originating from the 6^3D_2 level, also creates a temporary overpopulation in the 6^3P_1 level. The experimental error in the determination of the mercury vapour pressure corresponds to an uncertainty in the wall temperature of 1 – 2 °C.

The discharges were operated at DC current values of 1-10 mA for zero noble gas pressure and I : 0.1 – 1 mA for non-zero Ar pressures. At these currents the influence of electrophoretic and cataphoretic effects upon the axial number densities is negligible (Ken 38). The mercury vapour pressure ranged from 0.03 to 12 Pa, the Ar pressures were 133 and 400 Pa.

A dye laser, pumped by a pulsed nitrogen laser (Molelectron DL II 14 and UV 14, respectively) was used as a light source. The dye used to create the 10 ns dye laser pulse at 365.5 nm was 2-phenyl-5-(4-biphenyl)-1,3,4-oxadiazole (PBD). The spectral width of the pulse was 0.01 nm and its energy was 30 μJ . The fluorescence signals were detected with photomultipliers in combination with interference filters. The photomultipliers were connected with an oscilloscope for visual inspection of the fluorescence signals when tuning the dye laser to the correct wavelength. Finally, a boxcar integrator and an X-Y recorder were used to record the fluorescence signals.

II.3. Emission measurements

These measurements were made for the discharge tube with long side legs described in section II.1.

The intensities at the optically thin lines with $366.3 \leq \lambda \leq 579.1$ nm (see fig. 1.1) were measured along a chord through the axis of the tube at the axial coordinate z_1 . This was done with a two-lens system and a monochromator-photomultiplier combination (see fig. 2.1). The measured spectral line shapes were completely determined by the transmission function of the monochromator. The detection sensitivity was absolutely calibrated using a tungsten ribbon lamp, for which the emissivity data were taken from de Vos (Vos 54). Since the emitted light from the discharge is polarized (Ski 26) corrections were made for the polarization of the apparatus. Corrections were also made for the transmission of the tube walls, which was measured at the wavelengths studied. The axial inhomogeneity of the discharge was monitored at the 407.8 nm line using a moveable glass fibre.

REFERENCES

- Bor 79 E. N. Borisov, A. L. Osherovich and V. N. Yakovlev, *Opt. Spectr.* **47**, 109 (1979).
- Ken 38 C. Kenty, *J. Appl. Phys.* **9**, 765 (1938).
- Mit 71 A.C.G. Mitchell and M.W. Zemansky, 'Resonance Radiation and Excited Atoms', Cambridge University Press, Cambridge (1971) ch. 3.
- Ski 26 H. W. B. Skinner, *Proc. Roy. Soc. (London)* **A112**, 642 (1926).
- Vos 54 J. C. de Vos, *Physica* **20**, 690 (1954).
- Wei 85 P. van de Weijer and R.M.M. Cremers, *J. Appl. Phys.* **57**, 672 (1985)

III. The absolute Hg 6^1P_1 direct electron impact excitation cross section determined in a low-pressure Hg discharge

In this chapter we describe the determination of the absolute scale of the Hg 6^1P_1 direct electron impact excitation cross section in the positive column of a low-pressure mercury discharge. The discharge was studied spectroscopically in a regime where direct excitation and radiative decay are the dominant population and depopulation mechanisms of the levels. Using a dye laser absorption method we determined the number density of the Hg 6^1P_1 level in the steady state as well as its decay rate in the afterglow under various discharge conditions. From the data we deduced the excitation rates of the 6^1P_1 level. The electron densities and temperatures in the tail of the energy distribution were obtained from measurements of the radiances at optically thin lines with known excitation functions. With the shape of the excitation function of the 184.9 nm line given in the literature, its absolute scale is obtained from our data.

III.1. Principle of the method

Consider a level for which radiative decay is the dominant depopulation mechanism, while population is due to electron impact excitation from the ground state and radiative cascade from higher levels. For a transition at λ from this level we have by definition

$$n_u(\rho)A_\lambda = n_0 n_e(\rho) \int_{E_u}^{\infty} dE_e f(E_e) \left(\frac{2}{m_e}\right)^{1/2} E_e^{1/2} \sigma_\lambda(E_e) \quad (3-1)$$

Here n_u , n_0 , n_e are the number densities of atoms in the upper level at energy E_u , in the ground state and of electrons, respectively. The relative radial position in the discharge tube is $\rho = r/R$; A_λ is the transition probability for the line λ , $f(E_e)$ the electron energy distribution, m_e the electron mass, $\sigma_\lambda(E_e)$ is the optical excitation function of the line for excitation by electron impact on ground state atoms (Moi 68); n_0 and $f(E_e)$ are assumed to be independent of the radial position. Writing $\sigma_\lambda(E_e)$ as

$$\sigma_\lambda(E_e) = b_\lambda \bar{\sigma}_\lambda(E_e) \quad (3-2)$$

where b_λ is the absolute value of $\sigma_\lambda(E_e)$ at some fixed energy E_0 and $\bar{\sigma}_\lambda(E_e)$

the function normalized at E_0 , we obtain for a Maxwellian electron energy distribution with temperature T_e

$$n_u(\rho)A_\lambda = n_e n_c(\rho) b_\lambda \bar{K}_\lambda(T_e) \quad (3.3)$$

Here $\bar{K}_\lambda(T_e)$ is the rate coefficient for the normalized optical excitation. Measurement of the rate $n_u A_\lambda$ at a number of lines with known $\sigma_\lambda(E_c)$ then yields information on n_e and T_e . In fact, in this way essentially the electron density in the tail of the energy distribution is measured. Therefore, we define the quantity

$$n_{ct}(\rho) := n_e(\rho) e^{-\langle E \rangle / kT_e} \quad (3.4)$$

where $\langle E \rangle$ is the mean energy of the upper levels of the observed lines.

For an optically thin line the absolute radiance L_λ in a direction normal to the surface of the discharge tube is then given by

$$L_\lambda := \frac{R}{4\pi} \int_{-1}^1 d\rho n_u(\rho) A_\lambda = \frac{R}{4\pi} n_0 \bar{n}_{ct} b_\lambda e^{\langle E \rangle / kT_e} \bar{K}_\lambda(T_e) \quad (3.5a)$$

$$\text{with } \bar{n}_{ct} = \int_{-1}^1 d\rho n_{ct}(\rho). \quad (3.6)$$

We measured L_λ at ten optically thin lines with known $\sigma_\lambda(E_c)$ and therefore known b_λ and $\bar{K}_\lambda(T_e)$ - see fig. 1.1 - under conditions where the above assumptions are valid. From the set of ten equations (3.5a), the two unknown quantities \bar{n}_{ct} and T_e are then obtained by a least squares fit.

Equation (3.5a) cannot be applied as such to the 184.9 nm line because the latter is optically thick and radiation trapping determines to a large extent the angular distribution of the radiation leaving the tube. However, in the steady state it is still true that locally the electron impact excitation rate (including cascade) must equal the net radiative depopulation rate $\dot{n}_{6^1P_1}(\rho)_{rad}$. Here $n_{6^1P_1}(\rho)$ represents the population in the 6^1P_1 level. We thus have:

$$L_{184.9}^* := \frac{R}{4\pi} \int_{-1}^1 d\rho \dot{n}_{6^1P_1}(\rho)_{rad} = \frac{R}{4\pi} n_0 \bar{n}_{ct} b_{184.9} e^{\langle E \rangle / kT_e} \bar{K}_{184.9}(T_e). \quad (3.5b)$$

We now show how $L_{184.9}^*$ can be determined experimentally. The 6^1P_1

population can be expanded in eigenfunctions $f_j(\rho)$ of the radiative transfer problem (Tri 76). Each f_j decays with its own characteristic time constant τ_j , so that

$$n_{6^1P_1}(\rho)_{rad} = n_{6^1P_1}(0) \sum_{j=0}^{\infty} d_j \frac{f_j(\rho)}{\tau_j},$$

where d_j are the expansion coefficients. It follows that

$$L_{184.9}^* = \delta \frac{R}{4\pi} \frac{n_{6^1P_1}(0)}{\tau_0}, \quad (3.5c)$$

$$\text{with } \delta = \sum_{j=0}^{\infty} d_j \frac{\tau_0}{\tau_j} \int_{-1}^1 d\rho f_j(\rho).$$

The ratios τ_0/τ_j and the eigenfunctions $f_j(\rho)$ can be taken from the radiative transfer theory for pure Doppler line broadening (Tri 76), which gives a sufficiently good description at these low mercury densities (see chapter IV). The expansion coefficients d_j can be derived from a measurement of the radial profile $n_{6^1P_1}(\rho)$. A dye laser absorption method was used to measure the density $n_{6^1P_1}(\rho)$ in the steady state and its decay time constant τ_0 in the afterglow of the discharge.

Using the relative optical excitation function $\tilde{\sigma}_{184.9}(E_e)$ from the literature (Ott 74, McL 82) we obtained from the set of equations (3.5) the values for \bar{n}_{e1} , T_e and the absolute scale of $\sigma_{184.9}(E_e)$, represented by $b_{184.9}$.

III.2. Experimental results and analysis

III.2.1. Axial inhomogeneity

In order to derive the 6^1P_1 depopulation rates at z_1 from the axially averaged values, information is needed on the axial inhomogeneity. For this purpose we measured the axial variation of the emitted intensity at the optically thin 407.8 nm line for all discharge conditions. The 407.8 nm line was chosen since the ratio of the calculated excitation rates $\bar{K}_i(T_e)$ of the 407.8 nm and 184.9 nm lines varies only a few percent for $1.5 \leq T_e \leq 3.0$ eV. Therefore, we may assume that the 184.9 nm excitation rate varies proportionally to the 407.8 nm excitation rate. Moreover, we may even assume this

proportionality for the 6^1P_1 number density, because its decay is governed by radiation transport processes at the 184.9 nm line and may be assumed to be independent of the axial position. For the calculation of the ratio of the excitation rates we used the known functions $\bar{\sigma}_\lambda(E_c)$ (Jon 62, Ott 74).

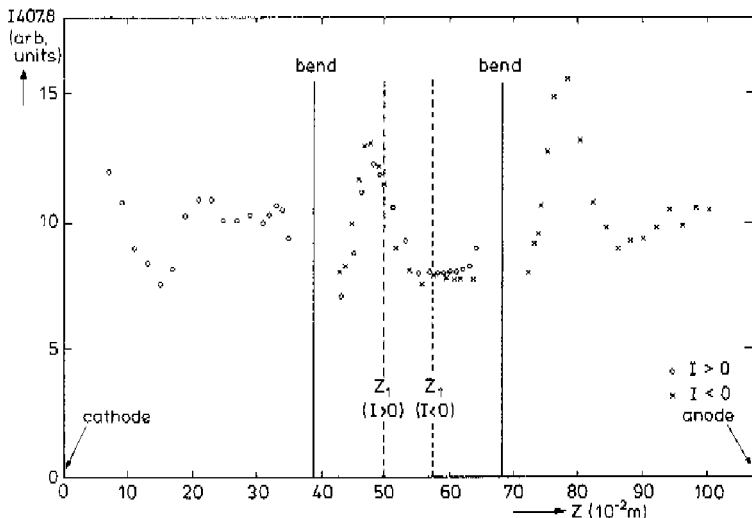


Fig. 3-1 Variation of the transversely emitted intensity $I_{407.8}$ along the axis of the discharge tube for $T_{Hg} = 40^\circ C$ and $I = 100$ mA. For both polarities of the discharge the cathode has been plotted at the left, the anode at the right. The position of the bends is indicated. The radiances at the optically thin lines were measured at z_1 , for $I > 0$. The radius of the discharge tube is $R = 12.5$ mm.

As an illustration $I_{407.8}(z)$ is shown (see fig. 3-1) for $T_{Hg} = 40^\circ C$ and $I = 100$ mA, where the inhomogeneous behaviour is the most pronounced. The intensity in the three straight parts of the discharge tube is plotted as a function of the distance to the cathode. The results are independent of the polarity of the discharge, which is shown in the figure for the central region of the tube. It is observed that about 10-20 μs after current reversal the inhomogeneous situation has reversed too. The effect is ascribed to the influence of the rectangular bend and the large mean free path of the electrons.

III.2.2. Density measurements

The 6^1P_1 number density measurements as well as the decay measurements using the dye laser absorption method were made at the nearly coincident

even isotope components of the 579.1 nm line (6^1P_1 - 6^1D_2). Thus the combined even isotopes were monitored (Mur 50). These represent 70% of the mercury in the natural abundance (Nie 50). Due to strong radiative coupling (chapters IV, V) the population in the 6^1P_1 hyperfine (h.f.) levels of the different isotopes is to a good approximation in natural abundance. This was checked experimentally by absorption measurements at the other h.f. components of the 579.1 nm line. The intensity of the laser beam was kept low enough (<0.5 mW) to avoid saturation effects.

The absorption profiles were evaluated using isotope shifts of Gerstenkorn *et al.* (Ger 71). The line shapes for the individual h.f. components were assumed to be Voigt profiles (Mit 71) with the Gaussian part given by the Doppler width and the Lorentzian part by the natural widths of the 6^1P_1 and 6^1D_2 levels. This was checked on the isolated hyperfine components α and α' for which the calculated line shapes agreed with the measured ones within a few percent. For the oscillator strength f of the 579.1 nm line we used the value $f = 0.25 (\pm 0.05)$ of van de Weijer and Cremers (Wei 83). Estimated

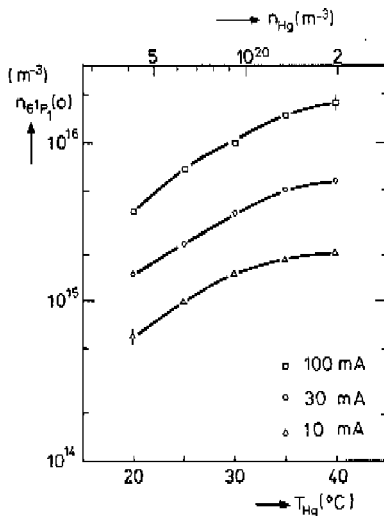


Fig. 3-2 Axial 6^1P_1 densities at z_1 as a function of the temperature T_{Hg} for the discharge currents $I = 10, 30, 100$ mA. The discharge tube radius $R = 12.5$ mm. An independent error of 20% in the vertical scale due to the error in the oscillator strength is not shown here.

corrections for the discharge behaviour at the ends of the middle section of the tube ("end effects") introduce an uncertainty of 5-10%. The 6^1P_1 densities at z_1 (see fig. 3.2) are then obtained from the axially averaged ones as discussed above. The corrections thus made increase with increasing discharge current, having extrema of -20% and +20% for the Hg temperatures 20°C and 40°C, respectively. The introduced error is 5-10%.

III.2.3. Radial profiles

In order to obtain the line integral $L_{184,9}^*$ of the 6^1P_1 depopulation rate along the chord through the axis of the tube, the 6^1P_1 radial profiles $n_{6^1\text{P}_1}(\rho)$ were measured. The experimental profiles $n_{6^1\text{P}_1}(\rho)/n_{6^1\text{P}_1}(0)$ are shown in fig. 3.3 for the current values 10, 100 mA and for the coldest spot temperatures ranging from 20°C to 40°C. Corrections were estimated for end effects and were small. The profiles are independent of the temperature and show a slight narrowing with decreasing discharge current. In our discharge regime the radial electron density profile becomes narrower with decreasing n_e due to the effects of space charges (Fra 76, chapter 4). For a radially independent T_e the radial excitation profile then becomes equally narrower.

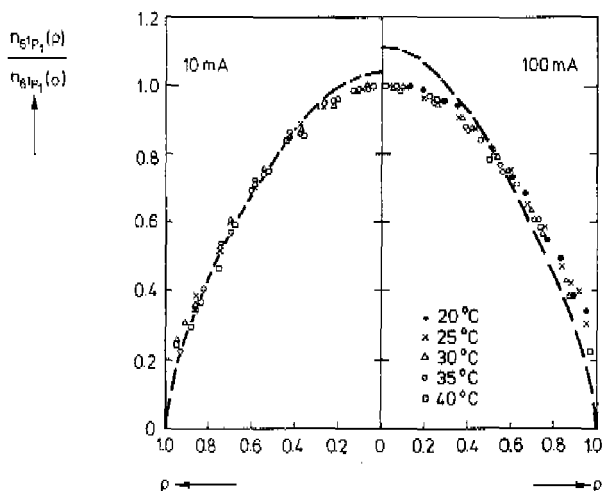


Fig. 3.3 Radial profiles of the 6^1P_1 density for $I = 10, 100$ mA and T_{Hg} varying from 20 to 40°C. The dashed curve shows the contribution of the lowest eigenmode of the radiative transfer problem for a Doppler line profile (see text).

that the dominant contribution to $L_{184,9}^*$ comes from the lowest eigenmode (see fig. 3-3). For the calculation of $L_{184,9}^*$ we have used the $f_j(\rho)$ and τ_0/τ_j for a Doppler line profile from van Trigt (Tri 76); see also chapter IV. The coefficient δ in eq. (3.5c) then amounts to 1.35, 1.38, 1.41 for the conditions with $I = 10, 30, 100$ mA, respectively. For a pure lowest eigenmode this would have been $\delta = 1.31$.

III.2.4. Decay measurements

The 6^1P_1 density decay curves, for which the shortest time constant is $1.5 \mu\text{s}$, were recorded for a time interval of $19 \mu\text{s}$ after the shortcircuiting of the discharge. The discharge voltage dropped to ~ 1 V within $\sim 0.2 \mu\text{s}$. The curves were stored in a computer data file. For these measurements the laser frequency was held at the maximum of the absorption coefficient κ_m of the

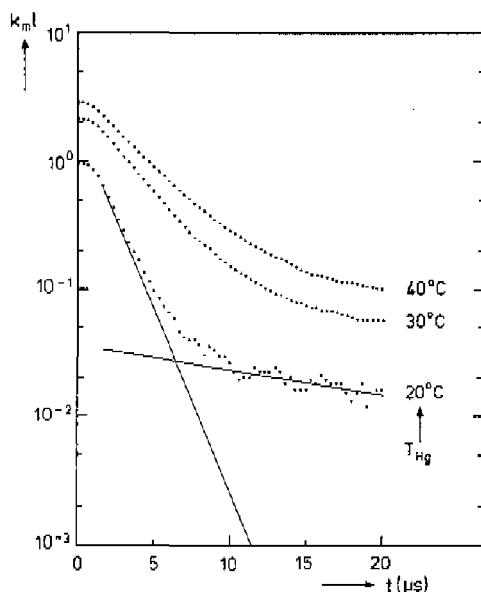


Fig 3-4 Time dependence of the optical depth $\kappa_m l$ measured along the axis of the discharge at the even isotope component of the 579.1 nm line ($6^1P_1 - 6^1D_2$); $I = 100$ mA, $T_{\text{Hg}} = 20, 30, 40$ °C. The solid lines represent the two exponentials obtained from the best fit for $T_{\text{Hg}} = 20$ °C. For $t \leq 1 \mu\text{s}$ the decay curves are affected by the finite sample time T_s ($1 \mu\text{s}$).

even isotope h.f. component. The resulting curves of $k_m(t)l$ for the current values of 100 mA are shown in fig. 3-4. The length of the sample time interval T_s (the aperture duration) of the boxcar was taken as $1.0 \mu\text{s}$.

After the energy input from the electric field has become zero the hot electrons are lost rapidly ($\tau_1 \sim 0.2 \mu\text{s}$) due to inelastic collisions with ground state Hg atoms (Pen 74). Their creation frequency in superelastic collisions of slow electrons with the long living 6^3P atoms is more than a factor of 100 smaller than at $t=0$, the moment of switch-off. Therefore, the direct excitation rate of the excited Hg states decreases very rapidly to a much lower level than in the steady state of the discharge. Measurements of the 365.0 nm emission showed that the population of the 6^3D_3 level, which has a natural lifetime of $\sim 7.4 \text{ ns}$ (Sem 77), dropped within $1.5 \mu\text{s}$ to 10% of its initial value. The shortest time constant of the remaining excitation rates will then be due to the decay of the electron density; $\tau_e \sim 10\text{-}20 \mu\text{s}$ (Fra 76, chapter 2). The 6^1P_1 density will decay with its effective radiative decay time constant to a new equilibrium value determined by the remaining excitation rates.

For the above reasons the $n_{6^1\text{P}_1}(t)$ decay curves were least squares fitted to a sum of two exponentials for times $t \geq 1.7 \mu\text{s}$. The two decay time constants

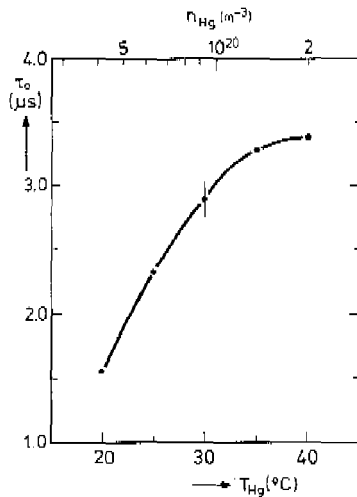


Fig. 3-5 Effective (radiative) decay time constant of the 6^1P_1 density as a function of the coldest spot temperature T_{Hg} which determines the mercury density n_{Hg} . Discharge tube radius $R = 12.5 \text{ mm}$.

found differed by at least a factor of ten in all cases. The resulting values for the shortest time constant τ_0 (see fig. 3.5) are independent of the discharge current (i.e. the electron density) in this regime. Due to the strong radiative coupling all 6^1P_1 h.f. levels of the different isotopes have the same decay time constant. The values of τ_0 increase with increasing mercury density which is caused by the radiation trapping (see chapter IV).

III.2.5. Experimental conditions

In our discharge conditions, population of the excited Hg levels is predominantly by electron impact excitation from the ground state and subsequent radiative cascades from higher levels (Kag 67, Wei 82). This is because the electron temperature is high ($T_e \sim 2\text{-}3$ eV) and the 6^3P densities ($n_{6^3P} \sim 10^{15}\text{-}10^{18} \text{ m}^{-3}$) and electron densities ($n_e \sim 10^{15}\text{-}10^{16} \text{ m}^{-3}$) are relatively low. For the 6^1P_1 level the contribution of excitation from the 6^3P levels to the measured 6^1P_1 decay rates is calculated at $\sim 3\%$ on the average with a maximum of 10%. For this calculation we used the above data of n_e , T_e , n_{6^3P} and our excitation cross sections $\sigma_{6^3P \rightarrow 6^1P_1}(E_e)$ (see appendix III). Using furthermore the results of Vriens and Smeets (Vri 80) it can be shown that electron impact depopulation rates are less than $\sim 5\%$ of the radiative decay rates for all levels studied ($< 1\%$ for 6^1P_1). Atomic collisional depopulation rates contribute less than $\sim 5\%$ for all these levels if cross section values $< 350 \cdot 10^{-20} \text{ m}^2$ are assumed ($30 \cdot 10^{-20} \text{ m}^2$ for the 6^1P_1 level, see also chapter V), which is reasonable.

It is well known that, in contrast with low-pressure noble gas discharges, the electron energy distribution in a Hg discharge with our pressure values is Maxwellian even in the tail of the distribution (Langmuir paradox) (Lan 24, 25; Vor 64, Ray 68, Mil 78a). The side legs of our discharge tube were made long enough to minimize the effects of hot electrons coming from the cathode (Vor 63). A Maxwellian electron energy distribution has been measured for our lowest T_{Hg} value in a nearly identical discharge tube (Kag 67). The electron temperature is furthermore independent of the radial position (Ver 61, Mil 78b). The influence of electrophoretic effects upon the axial mercury number densities is negligible at our low currents (Ken 38).

III.2.6. Optical excitation functions

For the ten emission lines used as a reference the optical excitation functions uncorrected for polarization effects (Moi 68) have been measured by

Jongerius (Jon 62) and Anderson *et al.* (And 67). Their normalized functions show good agreement but their absolute values b_λ , given at the electron energy of 15 eV, differ by -15% to +35%. Corrections for the polarization effects (Ski 26) were made using the data of Skinner and Appleyard (Ski 27), Heideman (Hei 64) and Heideman *et al.* (Hei 69). The shapes of the functions were taken from the detailed figures of Jongerius. For the 184.9 nm line the data for a natural isotope mixture were used (Ott 74). For $E_e \geq 15$ eV, $\sigma_{184.9}(E_e)$ has been taken constant, which introduces an error of $\sim 5\%$ in the absolute values obtained for $6.7 \leq E_e \leq 15$ eV.

It is difficult to express a preference for one of the two sets of absolute values. Recently Kaul (Kau 79) concluded from his absolute $\sigma_{253.7}$ measurements that the set of Anderson *et al.* must be preferred. However, recent experiments show that a structure at 8.8 eV is present in the direct excitation of the 6^3P_1 state emitting the 253.7 nm line (Kaz 80, Bar 81), as well as in its cascade population via the 7^3S_1 state at 435.8 nm (Shp 75). Jongerius's assumption in the derivation of the absolute $\sigma_{253.7}$ scale, that this structure in $\sigma_{253.7}$ was due completely to the cascade contribution $\sigma_{435.8}$ is therefore incorrect, but no conclusions can be drawn about his $\sigma_{435.8}$. For these reasons we use for the absolute values b_λ the mean values of the sets mentioned above.

III.2.7. Absolute cross section scale

The absolute radiances L_λ measured at z_1 in a direction normal to the surface and corrected for absorption by the tube walls are given in table III-1. The error is $\sim 10\%$. The values of $L_{184.9}^*$ at z_1 are also given. Apart from the independent error of 20% from the $f_{579.1}$ value, the error in $L_{184.9}^*$ is $\sim 15\%$. Using the branching ratio $A_{1014.0}/A_{407.8} = 6$ (And 67, Mos 78) it follows that the cascade contribution to $L_{184.9}^*$ is about 6% for all conditions.

The values of $\overline{n_{ei}}$ and T_e , as introduced in eqs. (3.4)-(3.6), obtained by the method described above, are given in table III-II. Here we have used $\langle E \rangle = 9.28$ eV. The uncertainty in T_e is fairly large ($\sim 35\%$): the fitting procedure is not very sensitive to T_e because all upper levels considered lie in a limited energy range of about 2 eV. The uncertainty in $\overline{n_{ei}}$ amounts to about 15%. Within the, relatively wide, error margins the present data are consistent with those of Kagan and Kasmaliev (Kag 67) obtained from the low energy part of $f(E_e)$ using Langmuir probes. Analysing our data with the b_λ set of Jongerius (Anderson *et al.*) instead of the average set yielded 15% smaller (larger) $b_{184.9}$ values.

T_{Hg} (°C)	20			25			30			35			40		
I (mA)	10	30	100	10	30	100	10	30	100	10	30	100	10	30	100
λ (nm)															
579.0/1	6.2	17.5	41	6.5	16.5	50	7.8	21	64	9.4	25	80	9.4	28	90
577.0	4.0	11.0	27	4.4	11.0	34	5.3	14.0	44	6.5	17.0	57	6.5	18.5	64
491.6	2.4	6.5	15.0	2.8	7.0	19.5	3.5	9.3	28	4.4	11.5	36	4.6	12.5	36
434.8	2.0	5.2	12.0	1.90	4.8	14.0	2.1	5.2	16.0	2.5	6.2	19.0	2.4	6.4	19.5
410.8	0.61	1.70	4.0	0.67	1.80	5.1	0.86	2.2	6.5	1.05	2.7	8.3	1.05	2.9	8.5
407.8	2.7	7.2	18.0	3.1	8.0	24	3.8	10.5	32	4.8	13.0	40.0	4.7	14.0	44
390.7	0.79	2.2	5.3	0.77	2.0	6.0	0.92	2.4	7.2	1.05	2.8	8.5	1.05	2.9	8.5
380.2	0.19	0.46	1.05	0.19	0.49	1.30	0.25	0.60	1.66	0.29	0.74	2.0	0.27	0.81	1.9
370.4	0.37	0.89	2.0	0.35	0.84	2.2	0.42	0.97	2.6	0.47	1.20	2.9	0.46	1.20	3.2
366.3	2.2	5.7	13.5	2.2	5.6	16.5	2.6	7.1	20.5	3.2	8.5	26	3.3	9.3	28
184.9	520	1300	3500	570	1400	4200	690	1700	4900	760	2100	6300	820	2300	7400

Table III-I The measured radiances at the optically thin lines, L_{λ} , and the quantity $L_{184.9}^*$ in units of $10^{15} \text{ m}^{-2} \text{ sec}^{-1} \text{ ster}^{-1}$ for the discharge conditions studied.

T_{Hg} (°C)	20			25			30			35			40		
I (mA)	10	30	100	10	30	100	10	30	100	10	30	100	10	30	100
$\bar{n}_{et}(10^{14} \text{ m}^{-3})$	1.3	3.5	8.3	0.92	2.3	6.8	0.76	1.9	5.8	0.62	1.6	4.8	0.43	1.2	3.5
T_e (eV)	4.4	3.9	3.6	3.5	3.3	3.1	3.2	2.8	2.6	2.9	2.7	2.3	2.8	2.6	2.2

Table III-II The values of the tail electron density \bar{n}_{et} and the electron temperature T_e obtained from the measured radiances.

The observed excitation rates are determined mainly by the values of $\sigma_{\lambda}(E_c)$ and $f(E_c)$ in the first few eV's above the upper level energies. Therefore, the obtained value of $\sigma_{184,9}(E_c)$ at 15 eV, $b_{184,9}$, is more sensitive to possible inaccuracies in the precise shape of the function than the value of the initial slope, $a_{184,9}$. For the shape of $\sigma_{184,9}(E_c)$ used (Ott 74) we have the relation $b_{184,9} (10^{-20} \text{ m}^2) = 6.0 a_{184,9} (10^{-20} \text{ m}^2/\text{eV})$. The values of the initial slope are important for use in analogous situations. The values at 15 eV are also given to allow a comparison with theoretical literature data from which these values can be obtained much more accurately than those of the initial slopes. The values obtained for $a_{184,9}$ and $b_{184,9}$ are shown in fig. 3-6. Apart

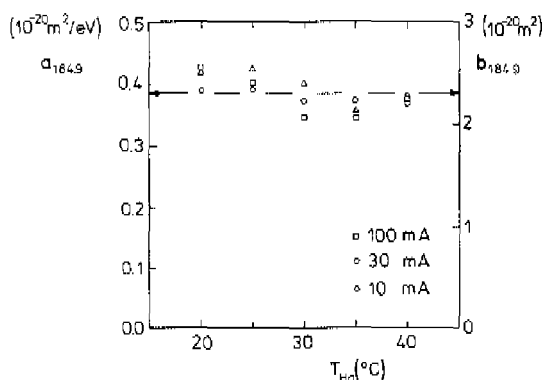


Fig. 3-6 Values of the initial slope of $\sigma_{184,9}(E_c)$, $a_{184,9}$, and of the excitation function at 15 eV, $b_{184,9}$, for the 15 discharge conditions studied.

from the independent error of 20% from the $f_{579,1}$ value, the error in these individual data is $\sim 35\%$, which is mainly due to the uncertainty in T_w .

The average values are

$$a_{184,9} = 0.38 \pm 0.1 \cdot 10^{-20} \text{ m}^2/\text{eV}$$

$$\sigma_{184,9} (15 \text{ eV}) = 2.3 \pm 0.6 \cdot 10^{-20} \text{ m}^2.$$

The error is 25% including the error in $f_{579,1}$. The excitation function $\sigma_{184,9}(E_c)$ approximated by four piecewise linear parts is shown in fig. 3-7.

The 6^1P_1 direct excitation cross section $\sigma_{6^1P_1}(E_c)$, which can be compared with literature data, is obtained from $\sigma_{184,9}(E_c)$ after subtraction of the cascade contribution $\sigma_{184,9\text{casc}}(E_c)$ (see fig. 3-7) with

$$\sigma_{184,9\text{casc}} (15 \text{ eV}) = 0.17 \pm 0.02 \cdot 10^{-20} \text{ m}^2.$$

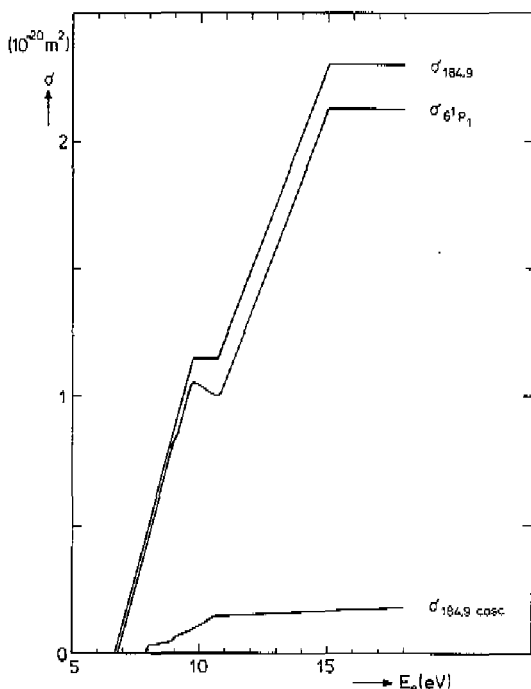


Fig. 3.7 The absolute optical excitation function $\sigma_{184,9}(E_e)$ and the absolute 6^1P_1 direct excitation cross section $\sigma_{6^1P_1}(E_e)$ obtained from this work. The uncertainty in the absolute scale is $\sim 30\%$. The shape of $\sigma_{184,9}(E_e)$ and the absolute cascade cross section $\sigma_{184,9 \text{ cascade}}(E_e)$ have been taken from literature (see text).

Here we used the value $A_{1014.0}/A_{407.8} = 6$ as mentioned above. It is seen from fig. 3.7 that this cascade contribution is less than 15% of $\sigma_{184,9}(E_e)$ for $6.7 \leq E_e \leq 15$ eV. The initial slope $a_{6^1P_1}$ in the energy region $6.7 \leq E_e \leq 9.7$ eV and the cross section value at 15 eV of the 6^1P_1 direct excitation cross section are

$$a_{6^1P_1} = 0.35 \pm 0.1 \cdot 10^{-20} \text{ m}^2/\text{eV},$$

$$\sigma_{6^1P_1}(15 \text{ eV}) = 2.1 \pm 0.6 \cdot 10^{-20} \text{ m}^2.$$

III.3. Comparison with literature

A comparison of the 6^1P_1 direct electron impact excitation cross section value at 15 eV with literature data is given in table III-III.

reference	Experiment			Theory	
	Arnot and Baines '35	Jongerius '62	This work	McConnell and Moisewitsch '68	Savchenko '70
$\sigma_{6^1P_1}(15 \text{ eV})$ (10^{-20} m^2)	4.2	0.3	2.1 ± 0.6	7.4	4.9

Table III-III Comparison of the 6^1P_1 direct excitation cross section at 15 eV, $\sigma_{6^1P_1}(15 \text{ eV})$, with experimental and theoretical literature data.

Arnot and Baines (Arn 35) used an electron scattering apparatus, measuring the scattered electrons over a wide angular range. Their value for $\sigma_{6^1P_1}$ at 15 eV is about a factor of 2 larger than ours. We note that their value for $\sigma_{6^1P_1}$ at 50 eV is a factor of 2.5 larger than the recent value of Kaul (Kau 79). From their energy resolution we conclude that they measured $\sum_0^{\infty} \sigma_{6^1P_1}(E_c)$, but at 50 eV this almost equals $\sigma_{6^1P_1}$ (McC 68). Jongerius (Jon 62) measured the relative function $\sigma_{184.9}(E_c)$ and obtained an absolute scale by assuming it to be equal to the cascade contribution for $6.7 \leq E_c \leq 12 \text{ eV}$. Calculation of $\sigma_{184.9 \text{ cascade}}(E_c)$ as given above would even decrease his absolute scale by a factor of 2. Since our results indicate that $\sigma_{184.9 \text{ cascade}}(E_c)$ is at most 15% of $\sigma_{184.9}(E_c)$ for $6.7 \leq E_c \leq 15 \text{ eV}$ (see fig. 3-7) it is clear why Jongerius's value is too small.

Of the theoretical data (Pen 32, Yav 47, McC 68, Sav 70) only the two most recent references are given since unfortunately in the older work some mathematical inaccuracies were made (McC 68). The scattering cross sections were calculated in the Born-Ochkur one-electron excitation approximation. Effects of configuration interaction with excited core configurations were neglected. The cross section shapes are in reasonable agreement with the one derived in this work (see fig. 3-7). The values at 15 eV are about a factor of 3 larger than our experimental value. The uncertainty estimated for the use of the Born-Ochkur approximation is a factor of 1.5-2 (Sav 70). Recent calculations of the oscillator strength of the 184.9 nm line (Sho 81) have shown that inclusion of core polarization gives a reduction of $f_{184.9}$ by approximately a factor of 1.6. Therefore, the use of the Born-Ochkur approximation together with the neglect of core polarization in the cross section calculations may be responsible for the difference between theory and experiment.

Appendix III

In this appendix we will make an estimate of the absolute cross sections for electron impact excitation of the Hg 6^1P_1 level from the $6^3P_{0,1,2}$ excited states: $\sigma_{6^3P \rightarrow 6^1P_1}(E_e)$. We will make use of the extensive experimental data available in literature for a DC Hg-Ar low-pressure discharge with tube radius $R = 18.0$ mm and 400 Pa argon pressure. For this discharge the 184.9 nm radiated power $P_{184.9}$, the electron density n_e and temperature T_e and the 6^3P number densities n_{6^3P} are known for the conditions $I = 400$ mA, $T_{Hg} = 11-80^\circ C$ and $T_{Hg} = 42^\circ C$, $I = 100-800$ mA (Koe 63, Ver 61, Koe 62). We make the assumption that $P_{184.9}$ is well described by electron impact excitation of the 6^1P_1 state from the ground state and from the excited $6^3P_{0,1,2}$ states. It can be shown that electron depopulation losses are always less than 10 percent of the total excitation rate for these discharge conditions.

The contribution to $P_{184.9}$ of the excitation from the ground state is calculated using our absolute optical excitation cross section $\sigma_{184.9}(E_e)$ obtained in section III.2. Deviations from the Maxwellian electron energy distribution have been taken into account using the two-electron group model in which the bulk and tail electrons are described with different temperatures T_e and T_1 , respectively (Lig 80). Using the values of T_1 (and T_e) given by these authors for the discharge conditions $T_{Hg} = 42^\circ C$, $I = 100-800$ mA it follows that the contribution to $P_{184.9}$ of direct excitation is about 10-20% in this range.

For the contribution to $P_{184.9}$ of the indirect excitation from the $6^3P_{0,1,2}$ states the shape of the excitation cross sections $\sigma_{6^3P \rightarrow 6^1P_1}(E_e)$ has been taken equal to the one for excitation of the 7^3S_1 state from the 6^3P states (Cay 50) which we have approximated by

$$\sigma_{6^3P \rightarrow 6^1P_1}(E_e) = \begin{cases} c(E_e - E_0) & , 0 \leq E_e - E_0 \text{ (eV)} \leq 1.5 \\ c \left\{ 1.5 + 0.7(E_e - E_0 - 1.5) \right\} & , 1.5 \leq E_e - E_0 \text{ (eV)} \leq 5.0 \text{ (3 \cdot A \cdot 1)} \\ 4c & , 5.0 \leq E_e - E_0 \text{ (eV)} \end{cases}$$

Here $E_0 = E_{6^1P} - E_{6^3P}$ and c is the initial slope given in units of $10^{-20} \text{ m}^2/\text{eV}$. The absolute scale of this cross section $\sigma_{6^3P \rightarrow 6^1P_1}(E_e)$ has been determined by equating the indirect 6^1P_1 excitation rate to the 184.9 nm output rate after subtracting the direct excitation rate. From the data for the condition $T_{Hg} = 42^\circ C$, $I = 600$ mA we obtain the value $c = 1.4 \cdot 10^{-20} \text{ m}^2/\text{eV}$. The effect

which the disturbance of the plasma by the probe has upon the measured electron densities is estimated to be 20 percent under these conditions.

Using the values for T_i/T_e and radial profiles for the Hg ground state density from a more refined discharge model (Lig 79) it is found that with this absolute scale for $\sigma_{6^3P \rightarrow 6^1P_1}(E_c)$ the $P_{134.9}$ data are described with a mean absolute deviation of 20% for the range of discharge conditions ($R = 18.0$ mm, $p_{Ar} = 400$ Pa) $T_{Hg} = 42^\circ\text{C}$, $I = 100$ -800 mA and $I = 400$ mA, $T_{Hg} = 11$ -80°C.

REFERENCES

- And 67 R. J. Anderson, E. T. P. Lee and C. C. Lin, *Phys. Rev.* **157**, 31 (1967).
 Arn 35 F. L. Arnot and G. O. Baines, *Proc. Roy. Soc. A* **151**, 256 (1935).
 Bar 60 B. T. Barnes, *J. Appl. Phys.* **31**, 852 (1960).
 Bar 81 K. Bartschat, C. F. Hanne, A. Wolcke and J. Kessler, *Phys. Rev. Lett.* **47**, 997 (1981).
 Cay 59 M. A. Cayless, *British J. Appl. Phys.* **10**, 186 (1959).
 Fra 76 R. N. Franklin, 'Plasma Phenomena in Gas Discharges', Clarendon, Oxford (1976).
 Ger 77 S. Gerstenkorn, J. J. Labarthe and J. Vergès, *Physica Scripta* **15**, 167 (1977).
 Hei 64 H. G. M. Heideman, *Phys. Lett.* **13**, 309 (1964).
 Hei 69 H. G. M. Heideman, C. Smit and J. A. Smit, *Physica* **45**, 305 (1969).
 Jon 62 H. M. Jongerius, *Philips Res. Rep. Suppl.* **2** (1962).
 Kag 67 Yu. M. Kagan and B. Kasmaliev, *Opt. Spectr.* **22**, 293 (1967).
 Kau 79 R. D. Kaul, *J. Opt. Soc. Am.* **69**, 150 (1979).
 Kaz 80 S. M. Kazakov, A. J. Korotkov and O. B. Sphenik, *Sov. Phys. JETP* **51**, 847 (1980).
 Ken 38 C. Kenty, *J. Appl. Phys.* **9**, 795 (1938).
 Koe 62 M. Koedam and A. A. Kruithof, *Physica* **28**, 80 (1962).
 Koe 63 M. Koedam, A. A. Kruithof and J. Riemens, *Physica* **29**, 565 (1963).
 Lan 24 I. Langmuir and H. Mott-Smith, *Gen. Electr. Rev.* **27**, 616 (1924).
 Lan 25 I. Langmuir, *Phys. Rev.* **26**, 585 (1925).
 Lig 79 F. A. S. Ligthart, *Bull. Am. Phys. Soc.* **24**, 186 (1979).
 Lig 80 F. A. S. Ligthart and R. A. J. Keijser, *J. Appl. Phys.* **51**, 5295 (1980).
 McC 68 J. C. McConnell and B. L. Moiseiwitsch, *J. Phys. B. (Proc. Phys. Soc.)* **1**, 406 (1968).
 McL 82 C. W. McLucas, H. J. E. Wehr, W. R. MacGillivray and M. C. Standage, *J. Phys.* **B15**, 1883 (1982).
 Mil 78a V. M. Milenin and N. A. Timofeev, *Sov. Phys. Tech. Phys.* **23**, 1048 (1978).
 Mil 78b V. M. Milenin and N. A. Timofeev, *Sov. Phys. Tech. Phys.* **23**, 1175 (1978).
 Mit 71 A. C. G. Mitchell and M. W. Zemansky, 'Resonance Radiation and Excited Atoms', Cambridge University Press, Cambridge (1971).
 Moi 68 B. L. Moiseiwitsch and S. J. Smith, *Rev. Mod. Phys.* **40**, 238 (1968).
 Mos 78 E. R. Mosburg and M. D. Wilke, *J. Quant. Spectr. Rad. Transfer* **19**, 69 (1978).
 Mur 50 K. Murakawa and S. Suwa, *J. Phys. Soc. Japan* **5**, 429 (1950).
 Nie 50 A. O. Nier, *Phys. Rev.* **79**, 450 (1950).
 Ott 74 T. W. Ottley, D. R. Denne and H. Kleinpoppen, *J. Phys.* **B7**, L179 (1974).
 Pen 74 N. P. Penkin and T. Redko, *Opt. Spectr.* **36**, 258 (1974).
 Pen 32 W. G. Penney, *Phys. Rev.* **39**, 467 (1932).
 Ray 68 S. W. Rayment and N. D. Twiddy, *Proc. Roy. Soc. A* **304**, 87 (1968).
 Sav 70 V. N. Savchenko, *Opt. Spectr.* **30**, 6 (1970).
 Sem 77 I. V. Semenova and Yu. M. Smirnov, *Opt. Spectr.* **42**, 477 (1977).
 Sho 81 P. Shorer, *Phys. Rev.* **A24**, 667 (1981).
 Sph 75 O. B. Sphenik, V. V. Souter, A. N. Zavitopulo, J. P. Zapesochnyi and E. E. Kontrosh, *Sov. Phys. JETP* **42**, 23 (1975).
 Ski 26 H. W. B. Skinner, *Proc. Roy. Soc. (London)* **A112**, 642 (1926).
 Ski 27 H. W. B. Skinner and E. T. S. Appleyard, *Proc. Roy. Soc. (London)* **A117**, 224 (1927).
 Tri 76 C. van Trig, *Phys. Rev.* **A13**, 726 (1976).
 Ver 61 W. Verwey, *Philips Res. Rep. Suppl.* **2** (1961).
 Vor 63 N.A. Vorob'eva, Yu. M. Kagan and V. M. Milenin, *Sov. Phys. Tech. Phys.* **8**, 423 (1963).
 Vor 64 N.A. Vorob'eva, Yu. M. Kagan, R. J. Lyagushchenko and V. M. Milenin, *Sov. Phys. Tech. Phys.* **9**, 114 (1964).
 Vri 80 L. Vriens and A. H. M. Smeets, *Phys. Rev.* **A22**, 940 (1980).
 Wei 82 P. van de Weijer and R. M. M. Cremers, *J. Appl. Phys.* **53**, 1401 (1982).
 Wei 83 P. van de Weijer and R. M. M. Cremers, *J. Appl. Phys.* **54**, 2835 (1983).
 Yav 47 B. M. Yavorskii, *Zh. Eksp. Teor. Fiz.* **17**, 315 (1947).

IV. Radiative transport at the 184.9 nm Hg resonance line. Theory

IV.1. General formulation

In this chapter we will derive an expression for the radiative decay rate β of a system of excited atoms in its fundamental mode. The expression is obtained for a homogeneous medium and applies for large optical thickness and a vast range of collision rates. The spectral relaxation rate is discussed and a condition is given for the existence of a fundamental mode in this regime. The analytical expression for β is given for a hyperfine structure of the line.

The partial redistribution theory starts from the transport equation given by Payne *et al.* (Pay 74) and uses an expression for the photon redistribution function (Zan 41, Hub 69, Omo 72, Nie 77, Vos 78, Unn 52, Hum 62, Pay 74) with an approximation first made by Jefferies and White (Jef 60).

IV.1.1. Transport equation

The transport equation for resonance radiation is given by (Pay 74)

$$\frac{\partial}{\partial t} N(\bar{\rho}, x, t) = -\gamma N(\bar{\rho}, x, t) + S(\bar{\rho}, x, t) + \gamma k_0 R \pi^{1/2} \int_{-\infty}^{+\infty} dx' \int_{\bar{\rho}} d\bar{\rho}' N(\bar{\rho}', x', t) \bar{R}(x', x) \frac{e^{-k(x')R|\bar{\rho}' - \bar{\rho}|}}{4\pi|\bar{\rho}' - \bar{\rho}|^2} \quad (4.1)$$

Here we have neglected the effects of quenching of the excited atoms or absorption by impurity atoms. Furthermore, $\bar{\rho} = \vec{r}/R$ is the reduced spatial position vector, where $2R$ is the characteristic dimension of the enclosure, i.e. the diameter for a sphere or cylinder and the thickness for a slab. The reduced frequency distance to the line centre ν_0 is given by

$$x = \frac{\nu - \nu_0}{\nu_0} \frac{c}{\bar{\nu}}, \quad \text{where } \bar{\nu} = (2kT/m)^{1/2}$$

and c , k , T , m have their usual meaning.

$N(\bar{\rho}, x, t) dx d\bar{\rho}$ is the number of excited atoms in $d\bar{\rho}$ at $\bar{\rho}$ at time t , which will emit photons into the photon frequency interval dx at x , and $dt \gamma N(\bar{\rho}, x, t) dx d\bar{\rho}$ represents the number of photons emitted in dt from

$d\bar{\rho}$ into interval dx at x . As excited atoms we thus take into account those atoms which absorbed a photon and those which are scattering a photon; γ is the reciprocal natural lifetime of the excited state. $S(\bar{\rho}, x, t) dx d\bar{\rho}$ is the number of excited atoms in $d\bar{\rho}$ at $\bar{\rho}$, which will emit in dx at x per unit time, created by processes other than absorption of photons from other parts of the system. The angle-averaged redistribution function $\bar{R}(x', x)$ is defined such that $\bar{R}(x', x) ds k_0 \pi^{1/2} dx$ represents the probability of a photon of frequency x' being absorbed (or scattered) while traversing a distance ds and being reemitted into dx at x . V is the volume containing the excited gas, $k(x) = k_0 \pi^{1/2} L_V(x)$ is the absorption coefficient and $L_V(x)$ is the normalized Voigt absorption line profile given by

$$L_V(x) = \frac{a_v}{\pi^{3/2}} \int_{-\infty}^{+\infty} dy \frac{e^{-y^2}}{a_v^2 + (x-y)^2}, \quad (4.2a)$$

with

$$a_v = \frac{\lambda_0 \gamma}{4\pi \bar{v}} (1 + \gamma_c / \gamma). \quad (4.2b)$$

Here

$$k_0 = \frac{\lambda_0^3 N_0 \gamma}{8\pi^{3/2} \bar{v}} \frac{g_2}{g_1}$$

and for resonance broadening we have for the elastic collision rate γ_c (Ber 69, Omo 68, Gay 74)

$$\gamma_c / \gamma = 0.904 \frac{g_2}{g_1} \frac{N_0 \lambda_0^3}{6\pi^2} \zeta, \quad (4.3)$$

where $\zeta = 1$ for exact resonance and $\zeta < 1$ for quasi-resonance as occurs in the case of hyperfine structure (Gay 74). N_0 is the number of atoms per unit volume, g_2 and g_1 are the statistical weights of the upper and lower level, respectively, and λ_0 is the wavelength at the line centre.

Furthermore we will use the normalized Doppler line profile $L_D(x)$

$$L_D(x) = \frac{e^{-x^2}}{\sqrt{\pi}}. \quad (4.4)$$

In the following we will distinguish between the line core ($|x| \leq x_c$) and the line wings ($|x| \geq x_c$). The transition frequency $x_c > 0$ is defined by the equality of the first two terms in the asymptotic expansion of $L_V(x)$, which

represent the Doppler and Lorentz contributions to $L_{\nu}(x)$:

$$\frac{1}{\sqrt{\pi}} e^{-x^2} = \frac{a_{\nu}}{\pi x_c^2} .$$

This yields for $a_{\nu} \ll 1$ in good approximation:

$$x_c^2 \approx \ln \left\{ \frac{\sqrt{\pi}}{a_{\nu}} \ln \left(\frac{\sqrt{\pi}}{a_{\nu}} \ln \frac{\sqrt{\pi}}{a_{\nu}} \dots \right) \right\} .$$

IV.1.2. Frequency redistribution function

The angle-averaged frequency redistribution function can be written as (Zan 41, Hub 69, Omo 72, Nie 77, Vos 78, Pay 74)

$$\bar{R}(x', x) = (1 - P_c) R_{II}(x', x) + P_c R_{III}(x', x) , \quad (4.5a)$$

where

$$P_c = \frac{\gamma_c}{\gamma + \gamma_c} \quad (4.5b)$$

is the probability that an elastic collision will destroy the correlation between the absorbed and reemitted frequencies in the rest frame of the atoms. The terms with P_c and $1 - P_c$ give the contribution from the fractions of absorbed photons being reemitted with and without a decorrelating collision before emission. The functions $R_{II}(x', x)$ and $R_{III}(x', x)$ obey the sum rule

$$\int_{-\infty}^{+\infty} dx R_{II,III}(x', x) = L_{\nu}(x'). \quad (4.6)$$

For the calculation of radiative decay rates with the use of eq. (4.1), the function $R_{II}(x', x)$ can be approximated by (Jef 60, Pay 74)

$$R_{II}(x', x) \approx L_{\nu}(x') \{ (1 - a(x')) L_D(x) + a(x') \delta(x' - x) \} , \quad (4.7a)$$

with $a(x) \approx 0$ for $|x| \ll x_c$ and $a(x) \approx 1$ for $|x| \gg x_c$.

The function $R_{III}(x', x)$ can be approximated by (Hum 62, Pay 74)

$$R_{III}(x', x) \approx L_{\nu}(x') L_{\nu}(x). \quad (4.7b)$$

In the following we will therefore use for the redistribution function $\bar{R}(x', x)$ the expression

$$\bar{R}(x', x) = L_V(x') \{ (1 - P_c) \{ (1 - a(x')) L_D(x) + a(x') \delta(x' - x) \} + P_c L_V(x) \} \quad (4.8)$$

The following aspects of the photon frequency redistribution can be noted from expression (4.8). The scattering probability of the incoming photons with the frequency x' is proportional to the full Voigt absorption line profile at x' . A fraction P_c of the scattering photons undergoes a decorrelating collision and is emitted according to the full Voigt line profile again. For this fraction we have complete redistribution. The other fraction, $1 - P_c$, of the scattering photons is redistributed by the process of coherent scattering on a velocity distribution of atoms. The first term of this contribution in eq. (4.8) denotes the full frequency redistribution in the core of the line ($x < x_c$ and $a(x) \approx 0$) by the Doppler motion of these atoms which scatter the photon resonantly. The second term expresses the frequency coherence in the wings of the line ($x > x_c$ and $a(x) \approx 1$) where the photons are scattered predominantly off-resonance by all atoms.

In the case of low collision rates, $P_c \ll 1$, there is a loose coupling between the line centre and the line wing. Photons scattering in the line centre are emitted only for a small fraction of P_c at frequencies in the wing of the line, where the medium becomes optically thin and the photons can escape. Photons scattering in the line wing are emitted for the fraction P_c at frequencies within the line core. The main fraction, $1 - P_c$, is emitted at its (incoming) wing frequency again. This frequency correlation in the line wing causes the coupling of the spatial and frequency dependence in the excited atom distribution $N(\rho, x, t)$. The effect of the δ -function approximation upon the calculated values of the decay rate will be discussed later (see section IV.3).

Using the redistribution function $\bar{R}(x', x)$ of eq. (4.8) in the transport equation (4.1), the essential redistribution mechanisms for the calculation of the radiative decay rate β are taken into account.

IV.1.3. Radiative decay rate

In this section we will derive an expression for the radiative decay rate β of a simply connected volume with convex boundary, when the system of excited atoms is in its fundamental mode, i.e. 'at late times'. This is quite different from the situation studied by Payne *et al.* (Pay 74), who calculated the early time escape rate of the resonance radiation in a slab geometry with an excited atom distribution at $t=0$ uniform over the midplane $y=0$, and zero

elsewhere. The eqs. (4.9)-(4.14) below are the local versions of the analogous equations given by Payne *et al.*, but with a more general formulation of the geometrical aspects.

The radiative decay rate is the rate at which the energy in the excited atom density decays by means of radiation transport. We define the local radiative decay rate $\beta(\vec{\rho}, t)$ as

$$\beta(\vec{\rho}, t) := - \frac{1}{N(\vec{\rho}, t)} \frac{\partial}{\partial t} N(\vec{\rho}, t) , \quad (4.9)$$

with

$$N(\vec{\rho}, t) := \int_{-\infty}^{+\infty} dx N(\vec{\rho}, x, t) . \quad (4.10)$$

Consider the situation where the non-radiative creation term $S(\vec{\rho}, x, t) = 0$ for $t > 0$. Integration of eq. (4.1) over x yields with eq. (4.9) for $t > 0$

$$\beta(\vec{\rho}, t) := \gamma \int_{-\infty}^{+\infty} dx F(\vec{\rho}, x, t) \eta(\vec{\rho}, \tau_x, x, t) . \quad (4.11)$$

Eq. (4.11) expresses $\beta(\vec{\rho}, t)$ as the integral over all frequencies of the normalized emission line profile

$$F(\vec{\rho}, x, t) := \frac{N(\vec{\rho}, x, t)}{N(\vec{\rho}, t)} , \quad (4.12)$$

weighted with the escape function

$$\eta(\vec{\rho}, \tau_x, x, t) := 1 - \int_V d\vec{\rho}' \tau_x \frac{e^{-\tau_x |\vec{\rho}' - \vec{\rho}|}}{4\pi |\vec{\rho}' - \vec{\rho}|^2} \frac{N(\vec{\rho}', x, t)}{N(\vec{\rho}, x, t)} . \quad (4.13a)$$

The function η for the net escape of photons with frequency x from the volume element $d\vec{\rho}$ at $\vec{\rho}$ depends for given $\vec{\rho}, x, t$ upon the optical thickness

$$\tau_x := k(x) R ,$$

and upon the spatial profile at frequency x

$$f(\dot{\rho}, x, t) := \frac{N(\dot{\rho}, x, t)}{N(\bar{0}, x, t)} \quad (4.14)$$

via the ratio

$$\frac{N(\dot{\rho}', x, t)}{N(\dot{\rho}, x, t)} = \frac{f(\dot{\rho}', x, t)}{f(\dot{\rho}, x, t)}$$

For later use we define

$$g(\dot{\rho}, \tau_v, x, t) := 1 - \eta(\dot{\rho}, \tau_v, x, t). \quad (4.13b)$$

From eq. (4.13) it follows that for $\tau_v \gg 1$ we have $\eta \ll 1$, whereas for $\tau_v \rightarrow 0$ we find $\eta \rightarrow 1$. For conditions of strong imprisonment only a small fraction of the emitted line profile $F(\dot{\rho}, x, t)$ is optically thin ($\tau_v < 1$), so that for not too strong variation of $N(\dot{\rho}, x, t)$ with $\dot{\rho}$ we find from eq. (4.11): $\beta(\dot{\rho}, t) \ll \gamma$.

In order to attain an expression for $\beta(\bar{\rho}, t)$ from eq. (4.11) we will concentrate next on obtaining an expression for the emission line profile $F(\dot{\rho}, x, t)$. For this purpose eq. (4.1) is transformed into an equation for $F(\dot{\rho}, x, t)$. Using eqs. (4.8)-(4.14) together with eq. (4.1) we find for $t > 0$

$$\begin{aligned} \frac{\partial}{\partial t} F(\dot{\rho}, x, t) = & -\alpha(\dot{\rho}, \tau_v, x, t) F(\dot{\rho}, x, t) \\ & + \gamma(1 - P_c) L_D(x) (1 - \beta(\dot{\rho}, t) / \gamma - \varepsilon(\bar{\rho}, t)) \\ & + \gamma - P_c \quad L_V(x) (1 - \beta(\bar{\rho}, t) / \gamma) \end{aligned} \quad (4.15)$$

$$\text{with } \int_{-\infty}^{+\infty} dx F(\bar{\rho}, x, t) = 1.$$

$$\text{Here } \varepsilon(\dot{\rho}, t) = \int_{-\infty}^{+\infty} dx a(x) g(\bar{\rho}, \tau_v, x, t) F(\bar{\rho}, x, t) \ll 1.$$

Eq. (4.15) is a differential equation for $F(\bar{\rho}, x, t)$ in which the second and third terms on the right-hand side act as source terms. These terms depend on time only very weakly through the small corrections $\beta(\bar{\rho}, t) / \gamma$ and $\varepsilon(\bar{\rho}, t)$, which we shall neglect henceforth ($\varepsilon(\bar{\rho}, t)$ is of the order $a_v / (\pi x_c)$ for $\tau_v > 1$).

The relaxation rate $\alpha(\bar{\rho}, \tau_x, x, t)$ of the spectral distribution $F(\bar{\rho}, x, t)$ is given by

$$\alpha(\bar{\rho}, \tau_x, x, t) = \gamma(1 - a(x)(1 - P_c)g(\bar{\rho}, \tau_x, x, t) - \beta(\bar{\rho}, t)/\gamma) . \quad (4.16a)$$

In the line wing, where $a(x) \approx 1$, we find from eq. (4.16a)

$$\alpha(\bar{\rho}, \tau_x, x, t) \approx \gamma P_c(1 - \eta(\bar{\rho}, \tau_x, x, t)) + \gamma \eta(\bar{\rho}, \tau_x, x, t) - \beta(\bar{\rho}, t) , \quad x > x_c \quad (4.16b)$$

or

$$\alpha(\bar{\rho}, \tau_x, x, t) = \gamma P_c + \gamma(1 - P_c)\eta(\bar{\rho}, \tau_x, x, t) - \beta(\bar{\rho}, t) , \quad x > x_c . \quad (4.16c)$$

It is seen from eq. (4.16) that in the line core, where $a(x) \ll 1$, as well as in the far wing of the line, where $\eta \approx 1$, the spectral relaxation rate attains its maximum value γ to first order in β/γ , independent of $\bar{\rho}, \tau_x, x, t$. This corresponds to complete Doppler redistribution and complete escape, respectively. For frequencies in between the core and the far wing of the line the situation is more complex. The expression (4.16b) shows three contributions to the relaxation rate α . The first one represents the relaxation internally in the spectrum at the spatial coordinate $\bar{\rho}$ due to decorrelating collisions. The second one denotes the relaxation by the net change in spectral density at the frequency x due to the interaction with the other volume elements. The third one corrects the relaxation rate obtained from the first two terms, for the decay rate of the total excited state density at $\bar{\rho}, t$ in order to obtain the *spectral* relaxation rate. In the limit of $P_c = 1$ the relaxation rate equals γ to first order in β/γ , independent of $\bar{\rho}, \tau_x, x, t$, due to the combined effects of decorrelating collisions and net spectral density change. In the limit of $P_c = 0$ the spectral relaxation rate is equal to $\gamma \eta(\bar{\rho}, \tau_x, x, t) - \beta(\bar{\rho}, t)$ since the only relaxation mechanism left at a given frequency x is interaction with the other volume elements at this frequency. This is e.g. equivalent to diffusion if $\tau_x \gg 1$.

For $0 < \eta < 1$, which one can ascribe to a not too strong variation of $N(\bar{\rho}, x, t)$ as a function of $\bar{\rho}$, it follows from eq. (4.16c) that α is always larger than the spectral relaxation rate corresponding to decorrelating collisions, $\gamma P_c - \beta(\bar{\rho}, t)$. This minimum value of α is attained in the near wing of the line when the optical thickness is so large that the relaxation rate $\gamma \eta$ can be neglected.

For $P_c = 0$ the different frequency intervals in the line wing act independently, whereas in the line core they are strongly coupled by the Doppler redistribution. In appendix IV.A.1 it is shown that for $P_c = 0$ a fundamental mode exists for every wing frequency interval separately (Dav 57) as well as

for the line core as a whole, with spatial profiles denoted by $f^\circ(\bar{\rho}, x)$ and $f_c^\circ(\bar{\rho})$, respectively. The superscript $^\circ$ denotes $P_c = 0$; no superscript is used for $P_c > 0$.

For $P_c > 0$ all frequency intervals are coupled. After a time sufficiently long for the $f^\circ(\bar{\rho}, x, t)$ and $f_c^\circ(\bar{\rho}, t)$ in the $P_c = 0$ case to be in their fundamental modes at all x , the spatial profiles for a non-zero small P_c value $f(\bar{\rho}, x, t)$ and so η , g and α vary in time only slowly. This slow variation in time is mainly due to a time dependence of the spectral distribution $F(\bar{\rho}, x, t)$, which is caused by the weak coupling of the different spectral regions. However, if the spectral relaxation rate $\alpha(\bar{\rho}, \tau_x, x, t)$ is much larger than the decay rate $\beta(\bar{\rho}, t)$ for a given $N(\bar{\rho}, t)$, the spectrum $F(\bar{\rho}, x, t)$ can accommodate itself quasi-instantaneously to the situation with the density profile $N(\bar{\rho}, t)$. In this case it is reasonable to assume that one fundamental mode exists, in which the spectrum $F(\bar{\rho}, x)$, the spatial profiles $f(\bar{\rho}, x)$ and therefore $\eta(\bar{\rho}, \tau_x, x)$, $g(\bar{\rho}, \tau_x, x)$ and $\alpha(\bar{\rho}, \tau_x, x)$ are time independent. Obviously, β then does not depend on time and position either and the decay is exponential with radiative decay rate β . The condition for the existence of a fundamental mode then follows from eq. (4-16c) if we use the fact that the lower limit of the relaxation rate α for photons in the wing is found where η is largest, i.e. at $x = x_c$ ($\tau_x \equiv \tau_c$). The condition becomes

$$P_c + (1 - P_c)\eta(\tau_c) \gg \beta/\gamma. \quad (4-17)$$

In this inequality we made the approximation

$\eta(\bar{\rho}, \tau_c, x_c) \approx \eta(\bar{0}, \tau_c, x_c) \equiv \eta(\tau_c)$. The unknown spatial profile $f(\bar{\rho}, x_c)$ at x_c is called $f(\bar{\rho})$, so that η at $\bar{\rho} = \bar{0}$ is only a function of τ_c . For the behaviour of $\eta(\tau_c)$ the precise spatial dependence of $f(\bar{\rho}, x_c)$ is of minor importance; see appendix IV.B.

The fundamental mode radiative decay rate β can be found in an iterative way by assuming a function $f(\bar{\rho}, x)$, so that the spectrum $F(\bar{\rho}, x)$ is to first order in β/γ obtained from eq. (4-15):

$$F(\bar{\rho}, x) = \frac{(1 - P_c)L_D(x) + P_c L_V(x)}{1 - (1 - P_c)a(x)g(\bar{\rho}, \tau_x, x)} \quad (4-18)$$

and by varying $f(\bar{\rho}, x)$ until the integral

$$\int_{-\infty}^{+\infty} dx F(\bar{\rho}, x) \eta(\bar{\rho}, \tau_x, x) = \beta/\gamma \quad \text{is independent of } \bar{\rho}. \quad (4-19)$$

In the case of a hyperfine structure with the strengths of the components d_i given by the natural abundance of the isotopes, an analogous calculation can be made. Taking proper account of the processes for the individual components through eqs. (4.12)-(4.18) we find for the fundamental mode radiative decay rate of a hyperfine structure (hfs) with a natural abundance distribution in the excited state population

$$\beta_{\text{hfs}} = \gamma \int_{-\infty}^{+\infty} dx \frac{\sum_i (1 - P_{c_i}) d_i L_{D_i}(x) + \sum_i P_{c_i} d_i L_{V_i}(x)}{1 - \sum_i a_i(x) \frac{\tau_x}{\tau_x} (1 - P_{c_i}) g(\tau_x, x)} \eta(\tau_x, x) . \quad (4.20)$$

Here we used detailed balance relations for the hyperfine structure-mixing collisions due to own gas and foreign gas atoms. The effect of multiplet-mixing collisions due to foreign gas atoms upon the strength of the fluorescence radiation has been treated in Nie 78. The symbols P_{c_i} , d_i , $L_{D_i}(x)$, $L_{V_i}(x)$, τ_x , $a_i(x)$ denote the same quantities as before, but for the h.f.s. component i ; $\tau_x = \sum_i \tau_{x_i}$. The calculation of $\eta(\vec{\rho}, \tau_x, x)$ and therefore of β is done at $\vec{\rho} = \vec{0}$ for convenience. We have defined $\eta(\tau_x, x) := \eta(\vec{0}, \tau_x, x)$.

It is instructive to write the expression (4.20) as

$$\beta_{\text{hfs}} = \beta_{\text{nc}} + \beta_c , \quad (4.21)$$

where the two terms β_{nc} and β_c denote the contributions to β_{hfs} arising from the source terms without and with a decorrelating collision before emission, respectively.

With increasing density the first term, β_{nc} , decreases, because the optical thickness increases. At low collision rates ($\gamma_c/\gamma \ll 1 \rightarrow P_c \ll 1$) the second term, β_c , increases with increasing density because also the collision rate and therefore P_c increases. Whereas at very low collision rates the decay rate is mainly determined by the Doppler redistribution - β_{nc} - in a large density range, above a certain density the collisional redistribution term β_c dominates. Therefore, if this occurs when P_c is still small, $P_c \ll 1$, a minimum is present in the decay rate β as a function of density. Moreover it follows that in this parameter range the assumption of complete redistribution - $P_c = 1$ in eqs. (4.18) and (4.20) - introduces a large overestimation of β (see chapter V).

IV.2. Application to an infinite cylinder

In this section various aspects of the radiative transport theory given in section IV.1. are considered in more detail. Furthermore the use of an approximate form of the radial profile $f(\bar{\rho}, x)$ is discussed, which considerably simplifies the calculation of β , at the expense of only a small error.

Whereas the expressions (4.1)-(4.20) are equally valid in plane, cylindrical and spherical geometry – the difference showing only in $\eta(\bar{\rho}, \tau_x, x)$ – we henceforth confine our attention to the case of an infinitely long cylinder. Some quantities to be discussed are calculated at the cylinder axis $\rho = 0$ for convenience, where ρ is the reduced radial coordinate.

IV.2.1. Spectral line shape

We first consider the spectrum $F(0, x)$. For simplicity reasons this is done for a one-component line. The spectrum $F(0, x)$ is shown in fig. 4.1 for the parameter set $k_0 R = 10^3, 10^4$, $a_v = 0.1$, $P_c = 10^{-3}, 10^{-2}, 10^{-1}, 1$. The radial profile $f(\rho, x)$ has been approximated by the frequency independent profile $f_D(\rho)$, which is the radial profile for complete redistribution and a Doppler line shape in the limit of large optical thickness (see appendix IV.A). The calculation of the escape function $\eta(\tau_x)$ in this case is described in appendix IV.B. For $a(x)$ in the approximation (4.7a) of the redistribution function $R_{11}(x', x)$ we used the function (Pay 74)

$$a(x) = 1 - L_D(x)/L_V(x). \quad (4.22)$$

Also plotted is the function $G(x) := (1 - P_c) L_D(x) + P_c L_V(x)$, which is the source function in eq. (4.15) to first order in β/γ and ϵ . For $P_c = 1$ we have $F(0, x) = G(x) = L_V(x)$, the full Voigt profile.

It is interesting to compare the spectrum $F(0, x)$ with the Voigt line profile $L_V(x)$, which is the line shape in thermodynamic equilibrium. With eq. (4.22) it is found from eq. (4.18) that in the line core $F(0, x)$ is equal to $L_V(x)$ in a good approximation for $x \ll x_c$ if $\eta \ll 1$. This is analogous to the results of previous calculations (Hol 47, Hol 51, Tri 76b). In the line wing, $x > x_c$, where the relaxation rate terms $\gamma\eta$ and γP_c compete, the spectrum $F(0, x)$ approaches $L_V(x)$ for those frequencies where the spectral relaxation is dominated by incoherent scattering, i.e. $\eta \ll P_c$. The relative deviation of $F(0, x)$ from $L_V(x)$ in this case is $(1 - P_c) \eta(\tau_x)/P_c$. These results apply for all ρ and can be interpreted as follows. At each scattering in the core of the line a spectral redistribution takes place, for a fraction $(1 - P_c)$ according to a

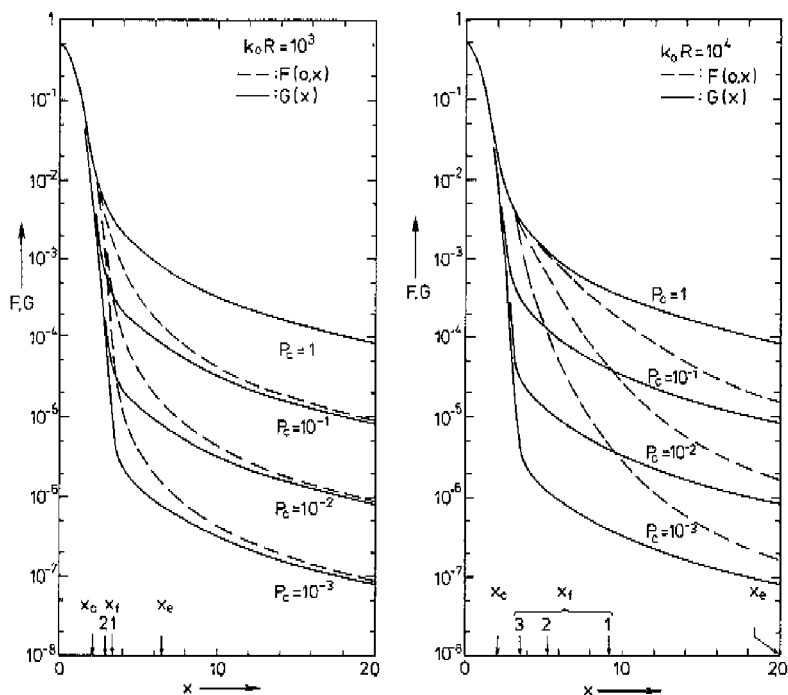


Fig. 4-1) The line shape functions $F(0, x)$ and $G(x)$ for a one-component line with $a_v = 0.1$, $P_c = 10^{-3}, 10^{-2}, 10^{-1}$, and the radial profile $f_D(\rho)$ (see text). For $P_c = 1$ we have $F(0, x) = G(x) = L_V(x)$, the full Voigt line profile. The frequencies x_c , x_f and x_e are also shown. The values of x_f for $P_c = 10^{-1}, 10^{-2}, 10^{-3}$ are denoted by the numbers 1, 2, 3, respectively. For $k_0 R = 10^3$ the values for $P_c = 10^{-2}$ and 10^{-3} nearly coincide. a. $k_0 R = 10^3$; b. $k_0 R = 10^4$.

Doppler and for a fraction P_c according to a Voigt profile. The latter fraction is the main source of supply of photons in the wing, $x > x_c$. For $\eta \ll P_c$ the photons will be trapped in the volume at fixed frequency until they eventually undergo an incoherent scattering. Consequently, a build-up of photon density in the near wing occurs to the full Voigt value, since on the average $1/P_c$ coherent scatterings will take place before an incoherent one. In the far wing, where the medium becomes optically thin ($\eta \approx 1$) no build-up exists and the spectrum approaches the source spectrum $G(x)$.

IV.2.2. Effective escape function

An interpretation closely related to the one in section IV. 2.1. can be given by writing the integrand of eq. (4-20) for the one-component line as

$$F(0, x) \eta(\tau_x, x) = G(x) \eta_{\text{eff}}(\tau_x, x) \quad (4-23)$$

with the effective escape function

$$\eta_{\text{eff}}(\tau_x, x) = \frac{\eta(\tau_x, x)}{1 - (1 - P_c) a(x) g(\tau_x, x)} \quad (4-24)$$

Whereas $\eta(\tau_x, x)$ can be looked upon as the probability for a photon to escape without undergoing any scattering at all, η_{eff} can be regarded as the probability that a photon escapes before undergoing a frequency changing scattering. In the line core $\eta_{\text{eff}}(\tau_x, x) = \eta(\tau_x, x)$, but in the near wing the effective escape function $\eta_{\text{eff}}(\tau_x, x)$ can be much larger than $\eta(\tau_x, x)$. This is due to the frequency correlation in the scattering process by which a wing

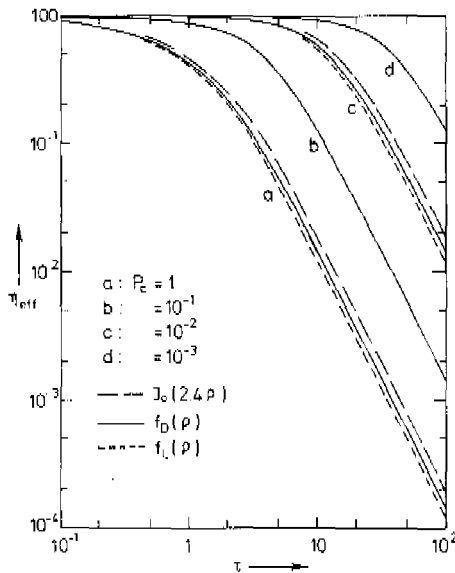


Fig. 4.2 The effective shape function $\eta_{\text{eff}}(\tau)$ for $P_c = 10^{-3}, 10^{-2}, 10^{-1}, 1$, $a(x) = 1$ and the radial profile $f_D(\rho)$. For $P_c = 10^{-2}, 1$ the curves calculated with the radial profiles $f_L(\rho)$ and $J_0(2.4\rho)$ are also shown. For the sake of the clarity $\eta(\tau)$ from eq. (4-29) is not shown here (see text).

photon at frequency x remains at x for many coherent scatterings before it is removed from its wing frequency in an incoherent scattering. In fig. 4.2, $\eta_{\text{eff}}(\tau_x, x)$ is plotted for $a(x) = 1$, several values of P_c and three choices of a frequency independent radial profile $f(\rho) = f(\rho, x)$, so that $\eta_{\text{eff}}(\tau_x, x)$ is only a function of the optical thickness τ at x : $\eta_{\text{eff}}(\tau)$; see appendix IV.B. Note that for $P_c = 1$ we have $\eta_{\text{eff}} = \eta$.

For use in the next section we define x_c as the frequency at which η reaches the value 0.5 and x_f as the frequency at which η_{eff} reaches that value. Simple relations can be derived for some quantities at the frequencies x_c and x_f . We find for the spectral density at x_c :

$$F(0, x_c) \cong \begin{cases} L_V(x_c) & , 0 < x_c < x_e \\ \frac{2}{1+P_c} P_c L_V(x_c) & , x_c < x_e \end{cases} \quad (4.25a)$$

$$\quad (4.25b)$$

For the escape function at x_f we find:

$$\eta_{x_f} := \eta(\tau_{x_f}, x_f) \cong \begin{cases} \eta(\tau_{x_c}, x_e) = 0.5 & , 0 < x_f \cong x_c < x_e \\ \frac{P_c}{1+P_c} & , x_c < x_f \leq x_e \end{cases} \quad (4.26a)$$

$$\quad (4.26b)$$

Using the relations (4.26) together with eq. (4.18) we find for the spectral density at x_f :

$$F(0, x_f) = \frac{G(x_f)}{2\eta_{x_f}} \cong \begin{cases} L_V(x_f) & , 0 < x_f \cong x_e < x_c \\ \frac{1+P_c}{2} L_V(x_f) & , x_c < x_f \leq x_e \end{cases} \quad (4.27a)$$

$$\quad (4.27b)$$

From eq. (4.26b) together with eq. (4.B.8) we obtain for $x_c < x_f \leq x_e$ the approximate relation between τ_{x_f} and P_c :

$$\tau_{x_f} \cong \frac{1.2}{\sqrt{P_c}} \quad (4.28)$$

IV.2.3. Integrand of expression for β

For the exact calculation of β the necessary solution for the radial profile $f(\rho, x)$ can be found by the iteration method discussed with eqs. (4.18), (4.19). Such a solution will not be attempted here to the full end. Rather we

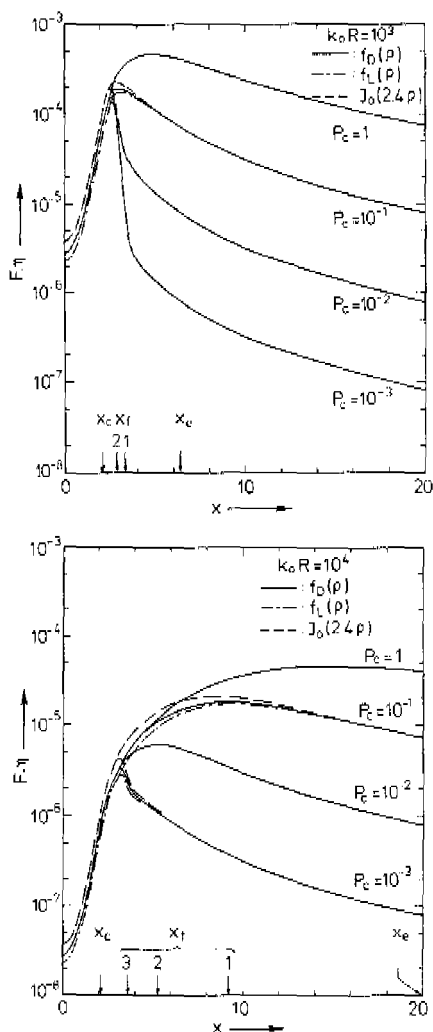


Fig. 4-3 The integrand of eq. (4-20), F_η , as a function of x for a one-component line with $a_v = 0.1$, $P_c = 10^{-3}, 10^{-2}, 10^{-1}, 1$ and the radial profile $f_D(\rho)$. For $P_c = 10^{-3}, 10^{-1}$ the curves calculated with the radial profiles $f_L(\rho)$ and $J_0(2.4\rho)$ are also shown. The frequencies x_c, x_t and x_e are also shown. The values of x_t for $P_c = 10^{-1}, 10^{-2}, 10^{-3}$ are denoted by the numbers 1, 2, 3, respectively. For $k_0 R = 10^3$ the x_t values for $P_c = 10^{-2}$ and 10^{-3} nearly coincide. a. $k_0 R = 10^3$; b. $k_0 R = 10^4$.

shall go through the first step of this scheme, i.e. we make a reasonable choice of $f(\rho, x)$, and show the relative insensitivity of β for the specific choice of $f(\rho, x)$.

For this purpose we next discuss the behaviour of the integrand (4.23) of the integral expression (4.20) for β . This integrand is plotted in fig. 4.3 for a one-component line, the same set of a_v , $k_0 R$, P_c as in fig. 4.1, and a few choices of a frequency independent radial profile $f(\rho)$, which are discussed in appendix IV.A.2. The values of x_c , x_e and x_f are also shown. It is seen that the integrand attains its maximum near x_f . This is analogous to the case of complete redistribution which is attained in our formalism as the special case of $P_c = 1$, giving $\eta_{\text{eff}} = \eta$ and $x_f = x_e$. Furthermore it is seen from fig. 4.3 that for the calculation of β , knowledge of the precise form of the radial profile $f(\rho, x)$ is mainly important for x near x_f .

To obtain an estimate of $f(\rho, x)$ near x_f , which can be used to a first approximation at all x in the calculation of the integrand, we will next discuss the radial profile $f(\rho, x)$.

IV.2.4. Radial profile

Using the expressions (4.12), (4.14), (4.16), (4.18) we find for the radial profile $f(\rho, x)$ in the fundamental mode

$$f(\rho, x) = \frac{\alpha(0, \tau_x, x) N(\rho)}{\alpha(\rho, \tau_x, x) N(0)} .$$

In the most general situation - $x_c < x_f < x_e$ - four spectral regions can be distinguished for $f(\rho, x)$:

- a. the core of the line: $0 < x < x_c$, $a(x) \ll 1$, $g = 1$;
 $f(\rho, x) \equiv f_c(\rho)$, independent of x , corresponding to complete Doppler redistribution.
- b. the near wing of the line: $x_c < x < x_f$, $a(x) \approx 1$, $g = 1$;
 $f(\rho, x) \approx f_c(\rho)$, independent of x , due to redistribution through incoherent scattering only.
- c. the middle wing of the line: $x_f < x < x_e$, $a(x) \approx 1$, $g \approx 1$;
 $f(\rho, x)$ is a function of x and is determined at each x by the (source) function $f_c(\rho)$ as well as by P_c and τ_x .
- d. the far wing of the line: $x > x_e$, $a(x) \approx 1$, $g \ll 1$;
 $f(\rho, x) \approx f_c(\rho)$, independent of x , since for the emitted photons the medium is optically thin.

The radial profile $f(\rho, x)$ is always broader than the diffusion profile $J_0(2.404\rho)$, and we assume $f(\rho, x_r)$ to be not much broader than $f_L(\rho)$ (see appendix IV.A). For the calculation of β we then approximate $f(\rho, x)$ at all x by $f_D(\rho)$, which lies in between $J_0(2.404\rho)$ and $f_L(\rho)$, in this way smoothly joining the regime of complete Doppler redistribution. Here $f_L(\rho)$ and $f_D(\rho)$ are the radial profiles for complete redistribution and a Lorentz and Doppler line profile, respectively.

For these frequency independent radial profiles the escape function at the cylinder axis only depends on the optical thickness τ_x : $\eta(\tau_x, x) = \eta(\tau_x)$. The calculation of $\eta(\tau_x)$ for the radial profiles $f_D(\rho)$, $f_L(\rho)$ and $J_0(2.404\rho)$ is described in appendix IV.B. The resulting curves of $\eta(\tau_x)$ are shown in fig. 4.2. Using the $\eta(\tau_x)$ functions for $f_D(\rho)$ and $f_L(\rho)$ in eq.(4.20) we have checked that for the case of complete redistribution ($P_c = 1$) and a one-component line in the limit of large optical thickness the analytical results of van Trigt (Tri 76a) for β are reproduced within 1% or better for any Voigt profile ($a_v \geq 0$). It has been shown by van Trigt (Tri 76a), that for a general Voigt line profile $L_v(x)$ and complete redistribution in frequency (eq. (4.20) with $P_c = 1$), values of β with 10% accuracy are obtained with $\eta(\tau_x)$ given by

$$\eta(\tau_x) = 1 - \frac{\tau_x}{5/8\pi} \arctan\left(\frac{5/8\pi}{\tau_x}\right). \quad (4.29)$$

The values of $\eta(\tau_x)$ from (4.29) are not shown in fig. 4.2 for the sake of clarity. For $\tau_x \leq 1.5$ they are larger than $\eta(\tau_x)$ for the radial profile $f_D(\rho)$, with a maximum difference of 5% at $\tau_x = 0.6$. For $\tau_x > 1.5$ they are smaller than $\eta(\tau_x)$ for $f_D(\rho)$, with a maximum absolute difference of 10%, independent of τ_x for $\tau_x > 3$.

The radiative decay rate β can now be calculated from eq. (4.20) using the escape function for $f_D(\rho)$. The error in β due to this approximation can be estimated from the results obtained with the escape functions for $J_0(2.404\rho)$ and $f_L(\rho)$.

IV.3. Discussion

Our use in the theory of the angle-averaged redistribution function limits its application to cases of strong imprisonment, where the absorbed emission comes nearly equally from all directions so that the emission is approximately isotropic. The redistribution function given in eq. (4.5) has been calculated

quantum-mechanically (Hub 69, Omo 72, Nie 77, Vor 78) for foreign-gas broadening in the rest frame of the atom. The expressions for $R_{II}(x', x)$ and $R_{III}(x', x)$ in the laboratory frame (Unn 52, Hum 62, Jef 60) are rather complicated. The more simple expressions (4.7a,b), used in our theory in chapter IV.1, are approximations. It is argued by Payne *et al.* (Pay 74) that, with γ_c/γ given by eq. (4.3) and using eq. (4.7b) for $R_{III}(x', x)$, eq. (4.5) should also hold for self-broadening. The approximation of $R_{III}(x', x)$ by eq. (4.7b) is best when used for large values of $|x'|$ or $|x|$ (Pay 74, Hum 62), i.e. at large optical thickness where the wings dominate the radiation transport process. For the wings of a h.f.s. of overlapping line components this approximation is even better justified than for a single line, because on the average the frequency distance to the line centre of the h.f. components is larger.

In the approximation of $R_{II}(x', x)$ by eq. (4.7a) the use of the first term requires strong imprisonment as well: $k_0 R > 50$ (Pay 74). The effect of the approximation of the second term by a $\delta(x' - x)$ function (Jef 60) is discussed in more detail in appendix IV.C. With this Jefferies-White approximation the decay rate β is underestimated if the line wing is optically thick and the collision rate low ($P_c \ll 1$). The introduced error in β is estimated in appendix IV.C to be largest when β_{nc} and β_c of eq. (4.21) are about equal, i.e. near the minimum in $\beta(n_{Hg})$. This is confirmed by our data in chapter V. From a rough estimation we find in appendix IV.C that, at the ground state density of the minimum in $\beta(n)$ in the experiment of chapter V with cylinder radius $R = 12.5$ mm and zero perturber gas pressure, the decay rate β is underestimated by about 30% when the JW approximation is used. We feel that the observed difference of max. 25% between experiment and theory around the minimum in $\beta(n_{Hg})$ (see chapter V) is due for at least a large part to the JW approximation in $R_{II}(x', x)$, although the good agreement with the estimated error is fortuitous because of the roughness of the estimation. The use of the JW approximation then predicts a somewhat too pronounced minimum in β as a function of density. This has also been found for the early time escape rate of Ar resonance radiation (Pay 74).

The range of P_c values where expression (4.20) applies is mainly determined by the condition (4.17) for the existence of a fundamental mode in the JW approximation. It can be shown that for $k_0 R > 50$ and $a_v \ll 1$ we have $P_c \gg \beta_c/\gamma$. We then find that condition (4.17) is satisfied if

$$(1 - P_c) \eta(\tau_c) \gg \beta_{nc}/\gamma \quad : \text{ for all } P_c, \text{ and if}$$

$$(1 - P_c) \eta(\tau_c) \not\gg \beta_{nc}/\gamma \quad : \text{ for } P_c \gg \beta_{nc}/\gamma.$$

For a single line component $\eta(\tau_c)$ can be easily estimated using $\tau_c \approx 0.1 k_0 R a_v$.

REFERENCES

- Abr 72 M. Abramowitz and I. A. Stegun, 'Handbook of Mathematical Functions', U.S. GPO, Washington D.C. (1972) p. 369.
- Ber 69 P. R. Berman and W. E. Lamb, Phys. Rev. **187**, 221 (1969).
- Dav 57 B. Davison, 'Neutron Transport Theory', Clarendon Press, Oxford (1957) ch. 1-8.
- Gay 74 J. C. Gay, J. Phys. **35**, 813 (1974).
- Gra 65 I. S. Gradshteyn and I. M. Ryzhik, 'Table of Integrals, Series and Products', Acad. Press, New York (1965), p. 92.
- Hol 47 T. Holstein, Phys. Rev. **72**, 1212 (1947).
- Hol 51 T. Holstein, Phys. Rev. **83**, 1159 (1951).
- Hub 69 D. L. Huber, Phys. Rev. **178**, 93 (1969).
- Hum 62 D. G. Hummer, Mon. Not. R. Astron. Soc. **125**, 21 (1962).
- Jef 60 J. Jefferies and O. White, Astrophys. J. **132**, 767 (1960).
- Nie 77 G. Nienhuis and F. Schuller, Physica **92C**, 397 (1977).
- Nie 78 G. Nienhuis, Physica **95C**, 266 (1978).
- Omo 68 A. Omont and J. Meunier, Phys. Rev. **169**, 92 (1968).
- Omo 72 A. Omont, E. W. Smith and J. Cooper, Astrophys. J. **175**, 185 (1972).
- Ost 62 D. E. Osterbrock, Astrophys. J. **135**, 195 (1962).
- Pay 74 M. G. Payne, J. E. Talmage, G. S. Hurst and E. B. Wagner, Phys. Rev. **A9**, 1050 (1974).
- Tri 76a C. van Trigt, Phys. Rev. **A13**, 726 (1976).
- Tri 76b C. van Trigt, Phys. Rev. **A13**, 734 (1976).
- Unn 52 W. Unno, Publ. Astron. Soc. Jap. **4**, 100 (1952).
- Unn 55 W. Unno, Publ. Astron. Soc. Jap. **7**, 81 (1955).
- Vos 78 D. Voslamber and J.-B. Yelnik, Phys. Rev. Lett. **41**, 1233 (1978).
- Zan 41 H. Zanstra, Mon. Not. R. Astron. Soc. **101**, 273 (1941).

Appendix IV.A

In this appendix the spatial profile $f(\rho, x)$ in the fundamental mode is discussed in more detail for the case of an infinitely long cylinder. For a plane or spherical geometry analogous expressions can be obtained.

IV.A.1. Consider in the redistribution function approximation of eqs.(4.5), (4.7), (4.8) the case where $P_c = 0$ and assume that a spatial distribution of excited atoms exists, created at $t=0$ in such a way that the spectral distribution is non-zero in the optically thick wings ($\tau_x \gg 1$). For $x > x_c$ this situation is completely analogous to the 'one speed' (or 'constant cross section') approximation in the neutron transport theory (Dav 57). The results of this theory show that the radial profile $f^\circ(\rho, x)$ for $0 < \rho < 1 - 1/\tau_x$ is given in good approximation by the solution of a diffusion equation with the boundary condition $f^\circ(1 + 0.71/\tau_x, x) = 0$. (The superscript \circ denotes the very special situation of $P_c=0$; no superscript is used for $P_c > 0$, as occurs in real physical situations).

Therefore, a fundamental mode exists for each $x > x_c$ independently, with the radial profile

$$f^\circ(\rho, x) = J_0\left(\frac{2.404}{1 + 0.71/\tau_x}\rho\right), \quad x > x_c, \quad 0 < \rho < 1 - 1/\tau_x. \quad (4.A.1a)$$

It follows that $f^\circ(\rho, x)$ is always broader than $J_0(2.404\rho)$, the fundamental mode diffusion profile with its first zero at the wall. For $\tau_x \gg 1$ the differences, however, are very small. For the line core an analogous situation would exist, were it not for the Doppler redistribution exerting a strong coupling for all x with $0 < x < x_c$. We therefore expect the line core to act as a whole in a fundamental mode behaviour with the radial profile $f_c^\circ(\rho)$ independent of x and given by

$$J_0(2.404\rho) \leq f_c^\circ(\rho) \leq J_0\left(\frac{2.404}{1 + 0.71/\tau_x}\rho\right), \quad x \leq x_c, \quad 0 < \rho < 1 - 1/\tau_x. \quad (4.A.1b)$$

IV.A.2. Now let P_c become non-zero, $P_c > 0$: then there exists a certain coupling between the different frequency intervals which will yield spatial distributions different from eq. (4.A.1). Because the $f^\circ(\rho, x)$ are for all x broader than $J_0(2.404\rho)$, this will remain valid for $f(\rho, x)$. In the line core $f_c(\rho)$ will become broader due to the coupling to frequency regions with broader $f^\circ(\rho, x)$. Because $f^\circ(\rho, x)$ is broader for larger x , it can be expected that the strongest influence on the broadening of $f_c(\rho)$ comes from $x = x_t$,

where $\eta_{\text{eff}} = 0.5$. This comes about since for $x > x_f$ the photons mostly escape before a frequency changing scattering occurs:

$\eta_{\text{eff}}(\tau_x, x) > \eta_{\text{eff}}(\tau_{x_f}, x_f) = 0.5$; moreover, their generation rate decreases: $G(x) < G(x_f)$. For $x_c < x < x_f$ the opposite is true. We then find

$$J_0(2.404\rho) \leq f(\rho, x) \leq J_0\left(\frac{2.404}{1+0.71/\tau_x}\rho\right), \quad 0 < x < x_f, \quad 0 < \rho < 1 - 1/\tau_x. \quad (4\cdot A\cdot 2)$$

Therefore, if $P_c \ll 1$ then $\tau_{x_f} \gg 1$ and $f(\rho, x_f)$ and $f_c(\rho)$ are given to a good approximation by the narrowest possible profile:

$f(\rho, x_f) = f_c(\rho) = J_0(2.404\rho)$. If P_c increases τ_{x_f} decreases, and $f_c(\rho)$ and $f(\rho, x_f)$ become broader.

To what extent $f_c(\rho)$ is broadened can be seen best from the situation of complete redistribution: $P_c = 1$, where τ_{x_f} is smallest, $\tau_{x_f} = \tau_{x_c} \approx 1$, and $f(\rho, x_f) = f_c(\rho) = f(\rho)$. In this case (Tri 76a) the spatial profiles $f_D(\rho)$ and $f_L(\rho)$ for a Doppler and Lorentz line shape, respectively, are both broader than $J_0(2.404\rho)$. However, $f_L(\rho)$ is only 10% larger than $f_D(\rho)$ except very close to the wall, whereas the fraction of emitted photons with $\tau_x \approx 1$ is much larger for a Lorentz than for a Doppler line shape. For a Voigt line shape $f_V(\rho)$ will be in between $f_D(\rho)$ and $f_L(\rho)$, depending on the values of a_v and $k_0 R$.

So we have found for the radial profile at x_f , $f(\rho, x_f)$:

- i. if $x_f > x_c$: $f(\rho, x_f) \approx f_c(\rho)$
in both limits of $P_c \ll 1$ and $P_c = 1$. We assume that it will not be much broader than $f_c(\rho)$ for all P_c values. In fact we will assume that $f(\rho, x_f)$ is not much broader than $f_L(\rho)$.
- ii. if $x_f = x_c < x_c$: $f(\rho, x_f) = f_c(\rho) = J_0\left(\frac{2.404}{1+0.71/\tau_{x_c}}\rho\right) < f_D(\rho)$,

since the broadening influence of line wing photons decreases.

- iii. if $x_f = x_c < x_c$: $f(\rho, x_f) = f_c(\rho) = f_D(\rho)$,
since the line wings are optically thin.

In all cases $f(\rho, x_f)$ is broader than $J_0(2.404\rho)$.

Appendix IV.B

Calculation of the escape function $\eta(\tau)$

In this appendix we will calculate the escape function $\eta(\tau)$ at the axis of an infinitely long cylinder for a given spatial profile $f(\bar{\rho})$

$$\eta(\tau) = 1 - \int_V d\vec{\rho}' \tau \frac{e^{-\tau|\vec{\rho}'|}}{4\pi|\vec{\rho}'|^2} f(\vec{\rho}') . \quad (4\cdot B\cdot 1)$$

In a coordinate system with the spherical coordinates ρ' , θ , φ (θ is the angle between $\vec{\rho}'$ and the cylinder axis and φ is the angle in the $\theta=\pi/2$ plane) and the origin at the cylinder axis, $\eta(\tau)$ can be written as

$$\eta(\tau) = 1 - \int_0^{\pi/2} d\theta \sin \theta \int_0^{1/\sin \theta} d\rho' \tau e^{-\tau\rho'} f(\rho' \sin \theta) . \quad (4\cdot B\cdot 2)$$

Here we have used the cylindrical symmetry of the problem, which implies that $f(\vec{\rho}')$ is an even function of $\rho : = \rho' \sin \theta$. The integral in (4·B·2) can be simplified by approximation of $f(\rho)$ by a power series of a large but finite number of terms. With the boundary conditions $f(0) = 1$ and $f(1) = 0$, we find

$$f(\rho) = \sum_{n=1}^{n_{\max}} a_{2n} (1 - \rho^{2n}) , \quad (4\cdot B\cdot 3a)$$

$$\sum_{n=1}^{n_{\max}} a_{2n} = 1 . \quad (4\cdot B\cdot 3b)$$

This gives

$$\eta(\tau) = \sum_{n=1}^{n_{\max}} a_{2n} \eta_{2n}(\tau) , \quad (4\cdot B\cdot 4)$$

with

$$\begin{aligned} \eta_{2n}(\tau) &= 1 - \int_0^{\pi/2} d\theta \sin \theta \int_0^1 d\rho \frac{\tau}{\sin \theta} e^{-\rho\tau/\sin \theta} (1 - \rho^{2n}) \\ &= \int_0^{\pi/2} d\theta \sin \theta I_{2n}(\tau/\sin \theta) , \end{aligned} \quad (4\cdot B\cdot 5a)$$

$$I_{2n}(\sigma) = \frac{(2n)!}{\sigma^{2n}} - \sum_{k=1}^{2n} \frac{(2n)!}{(2n-k)!} \frac{e^{-\sigma}}{\sigma^k} . \quad (4\cdot B\cdot 5b)$$

Equation (4·B·5b) was obtained from Gra 65.

In this way $\eta_{2n}(\tau)$ and therefore $\eta(\tau)$ can be obtained from eq. (4·B·5) by numerical quadrature. However, for small τ , i.e. small σ , and large n , loss of significant figures occurs due to cancellation of terms. By expansion of $e^{-\sigma}$ in its power series it can be shown that all terms with $\frac{1}{\sigma^k}$, $k > 0$ in $I_{2n}(\sigma)$ cancel, leaving

$$I_{2n}(\sigma) = \sum_{j=0}^{\infty} c_{2n,j}(-\sigma)^j, \quad c_{2n,j} = \sum_{l=0}^{2n-1} \frac{(-1)^l (2n)!}{(2n-1-l)!(j+1+l)!} \quad (4·B·6)$$

In the calculation of $\eta_{2n}(\tau)$, eq. (4·B·5b) was used for $\sigma \geq 1$ and eq. (4·B·6) for $\sigma < 1$. In the limit of large τ we find from eqs. (4·B·4) and (4·B·5):

$$\eta(\tau) = a_2 \eta_2(\tau) = \frac{4}{3} \frac{a_2}{\tau^2} \quad (4·B·7)$$

We are left with the determination of the power series which describe the radial profiles $f_D(\rho)$, $f_L(\rho)$ and $J_0(2.404\rho)$ sufficiently well. It turns out that these profiles can be approximated within less than 1% by the expression

$$f(\rho) = \sum_{n=1}^3 a_{2n}(1-\rho^{2n}) + (1 - \sum_{n=1}^3 a_{2n})(1-\rho^8),$$

with the coefficients a_{2n} given in table IV·B·1. The coefficients a_2 , which determine the behaviour of $\eta(\tau)$ for large τ , can be determined with good accuracy from van Trigt (Tri 76a) (f_D , f_L) and Abr 72 (J_0), respectively. The coefficients a_4 and a_6 were obtained by a least squares fit ($a_8 = 1 - a_2 - a_4 - a_6$).

	a_2	a_4	a_6	a_8
$f_L(\rho)$	0.8983	0.3028	-1.6008	1.3997
$f_D(\rho)$	1.0712	-0.0109	-0.7878	0.7275
$J_0(2.404\rho)$	1.4450	-0.5212	-0.0799	-0.0037

Table IV·B·1 Coefficients of the power series expansion $\sum_{n=1}^4 a_{2n}(1-\rho^{2n})$, for the radial profiles $f_D(\rho)$, $f_L(\rho)$ and $J_0(2.404\rho)$.

For use in section IV.2.2. we note that the curves of $\eta(\tau)$ shown in fig. 4-2 are described within 30% for all τ by the function

$$\eta(\tau) = \frac{1}{0.7\tau^2 + 1} \quad (4-B-8)$$

It is illustrative to see that the decay rate at large optical thickness τ for the $J_0(2.404\rho)$ radial profile obtained from eq. (4-B-7) and a_2 from table IV-B-1 is exactly equal to the rate ν_a obtained from the diffusion equation with boundary conditions:

$$\frac{d^2 f}{d\rho^2} + \frac{1}{\rho} \frac{df}{d\rho} + \frac{\nu_a R^2}{D} f = 0, \quad f'(0) = 0, \quad f(1) = 0,$$

and using $D = \frac{1}{3} \gamma/k^2(x)$ (the equivalence of the gas kinetic diffusion coefficient $D = \frac{1}{3} \lambda v$). We find

$$\eta \gamma = \nu_a = 1.926 \gamma / \tau_x^2.$$

Appendix IV.C

In this appendix the influence on the calculated decay rate due to the Jefferies-White approximation (Jef 60) in the redistribution function $R_{II}(x', x)$ is discussed in more detail.

For large optical thickness the function $R_{II}(x', x)$ can be approximately written as (Jef 60, Pay 74)

$$R_{II}(x', x) = L_V(x') \{ b(x', x) L_D(x) + a(x', x) L_D(x' - x) \}, \quad (4-C-1)$$

with $b(x', x) \approx 1$ and $a(x', x) \approx 0$ for $|x'| \ll x_c$ and further $b(x', x) \approx 0$ and $a(x', x) \approx 1$ for $|x'| \gg x_c$. As a function of $|x'|$, $a(x', x)$ rises from zero to unity for $|x'|$ near x_c , the rate of rise depending somewhat on $|x|$. The function $b(x', x)$ behaves complementarily. The function $L_D(x' - x)$ in the second term denotes the Doppler shift experienced in the non-resonant coherent scattering of the photons.

In the approximation first introduced by Jefferies and White (Jef 60) this function is approximated by the $\delta(x' - x)$ function and $R_{II}(x', x)$ is expressed by eq. (4-7a) (Jef 60, Pay 74). The function $a(x')$ in eq. (4-7a), which is better documented than $a(x', x)$, rises strongly for $|x'|$ near x_c , as is shown in Jef 60 (see also eq. (4-22)). In the JW approximation the wing photons can only

escape from the volume at their frequency of 'creation'. Thus the effects of one-dimensional diffusion in frequency space (Unn 55, Ost 62) from wing frequencies near x_c to more outward lying optically thinner frequency regions are neglected. This diffusion process occurs if $P_c \ll 1$ due to a finite mean frequency shift Δx_1 , which is inherent in the scattering term $L_D(x' - x)$ and because of the larger number of photons emitted with frequency nearer the line core. The mean frequency shift $\Delta x_1 \approx 0.7$ (Ost 62) acts as a mean free path in the diffusion in frequency space. The neglect of this diffusion process causes eq. (4.20) to underestimate the decay rate β .

In the following we will make as an example quantitative estimates related to the radiative decay rates at the Hg 184.9 nm line obtained in chapter V for the experimental conditions $R = 12.5$ mm, $p_{Ar} = 0$ Pa. For $x_c < x_c$ ($n_{Hg} < 3 \cdot 10^{19} \text{ m}^{-3}$) the photons emitted in the optically thin wings escape at first try and the approximation has no influence upon the calculated decay rate value.

For $x_c > x_c$ ($n_{Hg} > 3 \cdot 10^{19} \text{ m}^{-3}$) a large role in the radiation transport is played by photons in the wings, and the situation is more complicated.

Photons from two sources contribute to the decay rate β .

i. Photons created in decorrelating collisions (β_c).

Because the term $P_c L_V(x)$ in the source spectrum $G(x)$ is a slowly varying function of x in the wing and a large fraction of the escaping photons comes from x values where $\eta_{eff} \approx 1$, the error in β_c will not be large.

ii. Photons emitted by the Doppler redistribution (β_{nc}).

This term contributes potentially the largest error to β if the JW approximation is made. It is seen from the behaviour of the non-resonant coherent scattering term $a(x', x) L_D(x' - x)$ in eq. (4.C.1) that photons scattered by this mechanism to the optically thinner line wing mostly come from the frequency region $x > x_c$. For $x_c < x_f < x_c$ ($n_{Hg} > 3 \cdot 10^{19} \text{ m}^{-3}$) the error in β_{nc} increases with increasing mercury density, as long as $P_c \ll 1$. Therefore, the error in β will be largest when β_{nc} and β_c of eq. (4.21) are about equal ($n_{Hg} = 1.5 \cdot 10^{20} \text{ m}^{-3}$) as is confirmed by the data in chapter V (see fig. 5.3). With further increasing ground state density the error decreases fast. This is because on the one hand the diffusion length $\Delta x \approx \Delta x_1 / \sqrt{P_c}$ decreases (due to the increasing P_c value), whereas on the other hand the frequency distance $|x_f - x_c|$ to the effectively optically thin region increases. The chance that a photon will diffuse over a distance $|x_f - x_c|$, estimated roughly as

$$\exp \left\{ - \left(\frac{x_f - x_c}{\Delta x_1} \right)^2 P_c \right\},$$

is about 0.97 for $n_{\text{H}\beta} \approx 1.5 \cdot 10^{20} \text{ m}^{-3}$, but has decreased to about $1 \cdot 10^{-3}$ already at $n_{\text{H}\beta} = 6 \cdot 10^{20} \text{ m}^{-3}$.

An estimate of the error in β made using the JW approximation is rather difficult and has also to take into account the expressions used for $a(x')$, $R_{\text{II}}(x', x)$ and $R_{\text{III}}(x', x)$. From a rough estimation we find that the decay rate β at $n_{\text{H}\beta} = 1.5 \cdot 10^{20} \text{ m}^{-3}$ is underestimated by about 30% owing to the use of the JW approximation. For this estimation we assumed that in the real situation 50 percent of the Doppler redistribution photons emitted with $x > x_c$ diffuse into the line core and 50 percent into the line wing (i.e. using $\eta_{\text{eff}} = 0.5$ for $x > x_c$ in the β_{nc} term of eq. (4.20)). Here x_c of the h.f.s. was determined from the equality of the Doppler and Lorentz contributions to the Voigt line profile of the h.f.s..

V. Radiative transport at the 184.9 nm Hg resonance line. Experimental results and analysis

In this chapter we report measurements of the fundamental mode radiative decay rate for the 184.9 nm Hg resonance line (see fig. 5-1) over a large range of experimental conditions in a cylindrical geometry. In this range strong

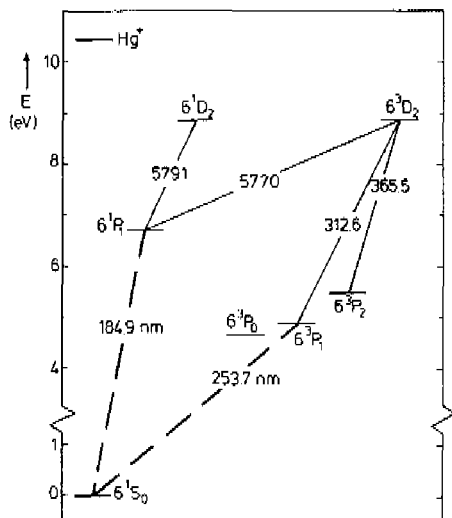


Fig. 5-1 Partial energy level diagram of mercury, showing the atomic transitions used in the dye laser absorption and the laser-induced fluorescence experiments (see text). Transitions indicated with solid (dashed) lines are optically thin (thick) for our experimental conditions.

radiation trapping occurs along with low collision rates and the theory described in chapter IV applies. The measurements were made using two different experimental methods. In both methods the decay of a temporary overpopulation in the Hg 6^1P_1 level was measured in a low-pressure Hg noble gas discharge. In the first method (section V.1) the overpopulation was obtained by the fast switch-off of the discharge. The decay of the Hg 6^1P_1 population in the afterglow of the discharge was measured using a dye laser absorption technique. In the second method (section V.2) the overpopulation was created in the steady state of the discharge by a dye laser pulse and the decay of its fluorescence at the 184.9 nm line was measured (laser-

induced fluorescence). Finally (section V.3), the experimental radiative decay rates are compared with those calculated from the theory of chapter IV.

V.1. Dye laser absorption measurements

The measurements with zero perturber gas pressure were performed at low currents. For the mercury noble-gas mixtures the measurements were also performed at high currents, which provided an extension of the radiative decay rate measuring range to larger mercury densities.

V.1.1. Zero perturber gas pressure

V.1.1.1. Decay measurements

For the 6^1P_1 density decay measurements the laser wavelength was held at the maximum of the absorption coefficient, k_m , of a hyperfine component of the 579.1 nm line ($6^1P_1 - 6^1D_2$) (Mur 50). Some examples of the resulting

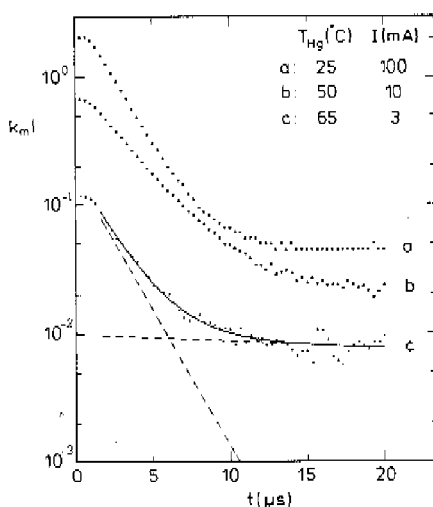


Fig. 5-2 Time dependence of the optical density measured along the cylinder axis for $T_{Hg} = 25, 50, 65^\circ\text{C}$ and $I < I_c$ (see text). The solid line represents the best fit of a sum of two exponentials for $T_{Hg} = 65^\circ\text{C}$, $I = 3$ mA; the dashed lines denote these two exponentials individually.

curves of $k_m(t)l$, the optical thickness along the discharge axis, are shown in fig. 5.2 for zero perturber gas pressure. For $t \leq 1 \mu\text{s}$ the decay curves are affected by the finite boxcar sample time ($1 \mu\text{s}$). We note here that the estimates entering the discussions below were based on literature data for the 6^3P densities (Wei 82), the electron density and energy distribution function (Kla 38, Sae 82), and the cross sections for electron impact (de-)excitation (Kle 21) at the atomic transitions $6^1\text{S}_0 - 6^3\text{P}_{0,1,2}$ (Lab 71), $6^1\text{S}_0 - 6^1\text{P}_1$ and $6^3\text{P}_{0,1,2} - 6^1\text{P}_1$ (chapter III). The decay curves will be discussed next.

At these low discharge currents the time dependence of the 6^1P_1 population in the afterglow is determined by its fundamental mode radiative decay rate β (see chapter IV), which we want to determine, as well as by the behaviour of the 6^1P_1 excitation. We note the following about this excitation. It can be estimated that after the discharge is switched off, the high energy tail (electron energy $> 5 \text{ eV}$) of the electron energy distribution cools off rapidly with a time constant $\ll 1 \mu\text{s}$ due to inelastic collisions with ground state Hg atoms. Therefore, the direct excitation of the excited Hg states decreases very rapidly to a level much lower than in the steady state of the discharge. This can be illustrated by measurements of the 365.0 nm emission from the very short-living 6^3D_3 level (natural lifetime $\sim 7.4 \text{ ns}$ (Sem 77)), which show a fast decay with time constant $\ll 1 \mu\text{s}$, followed after $\sim 2 \mu\text{s}$ by an order of magnitude slower decay. The 6^1P_1 level population $n_{6^1\text{P}_1}$, however, cannot follow the decreasing excitation instantaneously, because its decay time constant β^{-1} is too large ($> 1 \mu\text{s}$, see chapter III) due to radiation trapping. In this way an overpopulation is created at $t = 2 \mu\text{s}$.

For the description of $n_{6^1\text{P}_1}(t)$ at sufficiently low discharge currents, the remaining decreasing excitation for $t > 2 \mu\text{s}$ can be approximated well by an exponential function of time with rate $\beta_1 \ll \beta$. The radiative deexcitation for $t > 2 \mu\text{s}$ can be described by the fundamental mode radiative decay rate β (see chapter IV). This is because the radial dependence of the 6^1P_1 excitation and therefore of the 6^1P_1 density in the steady state of the discharge is already a good approximation to that of the fundamental mode radiative deexcitation rate. This was confirmed by measurements of the radial 6^1P_1 density profile; see also chapters III, IV. Because the same applies in the afterglow, the 6^1P_1 density decay curves are given simply as the sum of two exponentials with rate constants β and β_1 , respectively (Gem 75).

V.1.1.2. Radiative decay rate

The values of β and $\beta_1 \ll \beta$ were obtained from a least squares fit of a sum of two exponentials to the measured $n_{6^1\text{P}_1}(t)$ curves for $t \geq 2 \mu\text{s}$ (see

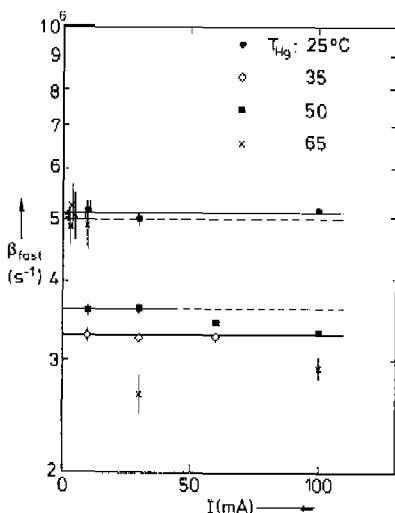


Fig. 5.3 The experimental fast decay rate as a function of the discharge current I for $T_{\text{Hg}} = 25, 35, 50$ and 65°C .

fig. 5.2), and differed by at least a factor of 10 under all conditions. At a given mercury density n_{Hg} , β was measured as a function of the current I , and was found to be independent of I at currents below a certain current $I_c(n_{\text{Hg}})$; see fig. 5.3. I_c decreases with increasing n_{Hg} and is for $R = 12.5$ mm larger than 100 mA at mercury densities less than $3 \cdot 10^{20} \text{ m}^{-3}$; see also chapter III. Estimates show that in this current region more than 90 percent of the 6^1P_1 excitation in the steady state of the discharge is due to direct excitation from the 6^1S_0 ground state. It follows from the discussion above that this yields a large overpopulation at $t \approx 2 \mu\text{s}$ (see fig. 5.2). Therefore, the approximation of the slow decay of the remaining 6^1P_1 excitation by an exponential curve of the same radial dependence as the density in the fundamental mode has only a small influence on the accuracy of the 'fast' β values obtained. The values of β , measured at $I < I_c(n_{\text{Hg}})$, are shown in figs. 5.4 and 5.5 as a function of the mercury density $n_{\text{Hg}}(T_{\text{Hg}})$ for several values of R .

The uncertainty of the data is 5%, except at the largest mercury density measured, where it is 20%. At still larger mercury densities the error increased drastically, and no data are presented. This increase is caused by a decreasing I_c and a decreasing 6^1P_1 density as a consequence. Moreover, discharge instabilities are present at these low current densities (1 A/m^2).

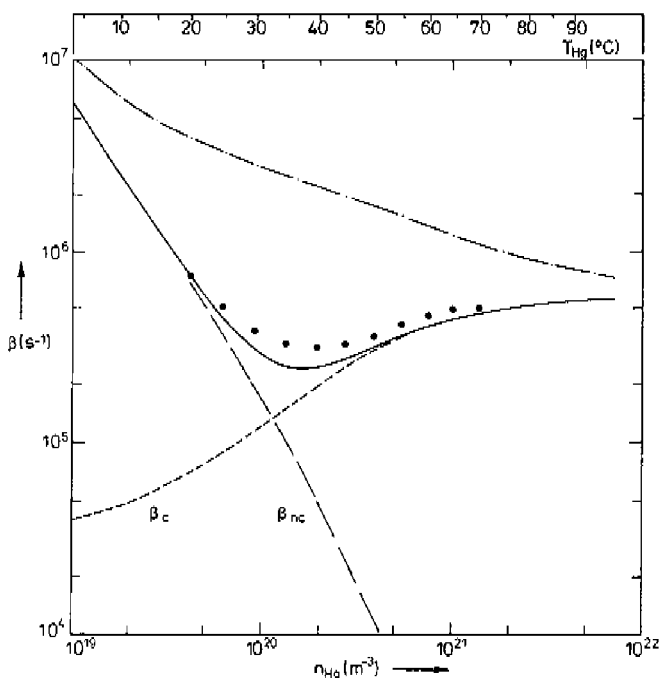


Fig. 5-4 The fundamental mode radiative decay rate β of the Hg 184.9 nm line as a function of the Hg number density n_{Hg} and the coldest spot temperature T_{Hg} . The cylinder radius is $R = 12.5$ mm. \bullet : experiment. — : partial frequency redistribution theory of chapter IV, eq. (4-20) with radial profile $f_D(\rho)$; $\beta = \beta_{\text{nc}} + \beta_{\text{c}}$; see text; theory with assumption of complete frequency redistribution (Tri 76): - - - . Both calculations were made for a natural abundance in the 6^1P_1 excited state.

Estimates show that electron impact depopulation rates are less than 1% of the radiative decay rates β . Atomic collisional depopulation rates contribute less than 1% if cross section values $< 0.05 \cdot 10^{-20} \text{ m}^2$ are assumed, which seems reasonable (Mas 71) in view of the large energy differences encountered in deexciting the 6^1P_1 level (see fig. 5-1). Effects of quenching by impurities are negligible since these are removed by the cleaning effect of the discharge (Ken 45). Spectroscopically no trace of impurities could be detected during the measurements. All 6^1P_1 hyperfine (h.f.) levels of the different isotopes (Leb 74) have the same decay rate β and, with the possible exception of the ^{204}Hg isotope which will be discussed in section V.3, their population is to a good approximation in accordance with the natural abundance (Nie 50). This is due to the strong radiative coupling (see fig. 5-6) and was confirmed

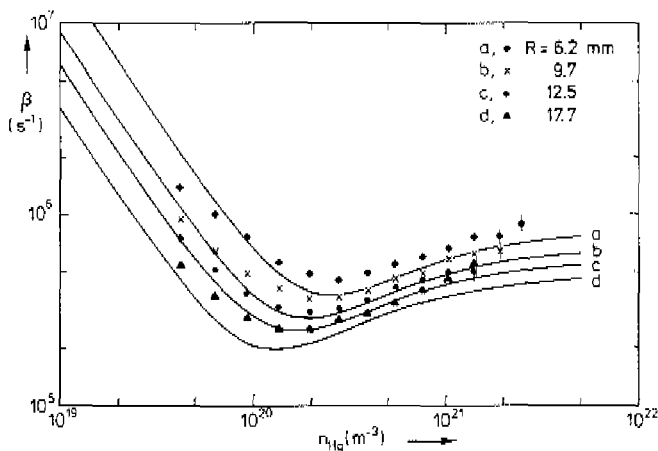


Fig. 5-5 The fundamental mode radiative decay rate β of the Hg 184.9 nm line as a function of the Hg number density n_{Hg} for various values of the cylinder radius R and zero perturber gas pressure. The experimental data were obtained using the dye laser absorption method. — : theory of chapter IV for a natural abundance in the Hg 6^1P_1 population.

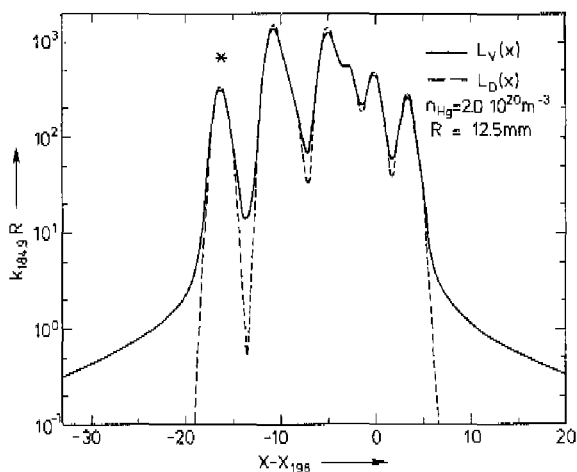


Fig. 5-6 Absorption coefficient hyperfine structure of the Hg 184.9 nm resonance line for a Voigt line and a Doppler line profile of the individual components. The asterisk denotes the ^{204}Hg line component. The other components represent the isotopes with mass number 202-196.

by absorption measurements at the other h.f. components of the 579.1 nm line (for h.f.s., see Mur 50).

The β values for $R = 12.5$ mm and $4 \cdot 10^{19} \leq n_{\text{Hg}} \leq 2 \cdot 10^{20} \text{ m}^{-3}$ agree with those of chapter III when allowance is made for a systematic error of $\sim 10\%$ in the latter data. This error arose from the tube construction at the ends of the middle section of the tube ('end effects') and was almost absent in the present experiment. In the work of this chapter we measured β in a much wider range of mercury densities (see fig. 5-4).

The radiative decay rate β as a function of the mercury density n_{Hg} , $\beta(n_{\text{Hg}})$, shows a pronounced minimum. The minimum value is about 60 percent of the value at the largest mercury density measured. A minimum in $\beta(n)$ of the fundamental mode, i.e. 'at late times', has only been observed for the Ne resonance line at 73.6 nm (Phe 59). The early time escape rate at the 104.8 nm Ar resonance line observed under special experimental conditions also showed a minimum which, however, was less pronounced (Pay 74). We also calculated β for a natural abundance density distribution in the excited (6^1P_1) state using the complete redistribution theory of van Trigt (Tri 76) for a Voigt line profile and the hyperfine structure of Leb 74 and Nie 50. These β values, shown also in fig. 5-4, can be about a factor of 8 larger than our experimental ones and show no minimum as a function of n_{Hg} . The occurrence of a minimum in $\beta(n_{\text{Hg}})$ in a density range where the Voigt absorption line profile varies only slightly, clearly shows that β is not a function of the optical thickness at line centre and of the absorption line shape only. This is in marked contrast with the complete redistribution formulation. In section 5.3 the experimental decay rates will be compared with calculated ones from the theory described in chapter IV.

The mercury density at which the minimum occurs, n_{Hgmin} , increases with decreasing R . It was shown in chapter IV that for $n_{\text{Hg}} \ll n_{\text{Hgmin}}$ the behaviour of β is mainly determined by the Doppler redistribution in the line core, whereas for $n_{\text{Hg}} \gg n_{\text{Hgmin}}$ it is dominated by the collisional redistribution in the wings of the line. This explains the different dependence of β upon R for $n_{\text{Hg}} \ll n_{\text{Hgmin}}$ and $n_{\text{Hg}} \gg n_{\text{Hgmin}}$. We note that β at different R values can be obtained easily from our data by interpolation, because it is found that β as a function of R at constant n_{Hg} shows a straight line on a double-log scale for all n_{Hg} measured; see fig. 5-7.

V.1.2. Mercury noble-gas mixtures

The influence upon β of a perturber gas (argon) added to the varying mercury pressure was measured for $R = 17.7$ mm. For these Hg-Ar dischar-

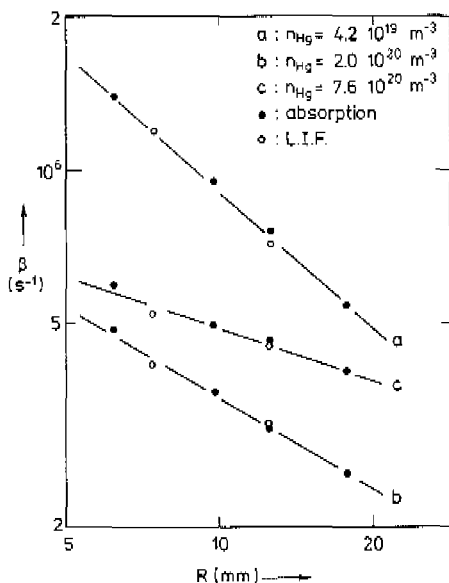


Fig. 5-7 The radiative decay rate β of the Hg 184.9 nm line as a function of the discharge tube radius R for various values of the mercury density n_{Hg} . The experimental data were obtained using two different experimental methods.

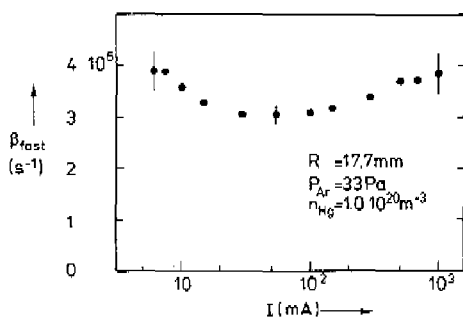


Fig. 5-8 The fast decay rate β_{fast} of the Hg 6^1P_1 density decay as a function of the discharge current for a Hg-Ar gas mixture. The decay rate was obtained at all currents from a least squares fit of a sum of two exponentials to the measured decay curves (see text).

ges with Ar pressures $p_{Ar} = 33$ and 67 Pa, we evaluated the 6^1P_1 density decay curves with a two-exponential sum function for currents up to 1 A. As an example values obtained for the rate representing the fast decay are shown in fig. 5.8 as a function of current. The following remarkable behaviour is noted

- i. at sufficiently low current values the fast decay rate is independent of the current, as was found for zero noble gas pressure.
- ii. at intermediate currents the fast decay rate obtained in this way is lower than the value at low currents and varies with the current.
- iii. at high currents ($I > 500$ mA) the fast decay rate obtained in this way is again independent of the current. Furthermore, the values differ less than 5 percent from the β values obtained from the low current data.

In our opinion this behaviour can be understood as follows. At the low Ar pressures used the 6^1P_1 level is populated at low currents most likely from the ground state and at high currents from the 6^3P states (Kag 68, Ver 61, Koe 62), as is the case for zero Ar pressure (see section V.1.1.). After the switch-off of the discharge the high energy electrons ($E_e > 5$ eV) relax fast ($\tau_h \ll 1 \mu s$) due to inelastic collisions with ground state atoms (see sections III.2.4 and V.1.1). However, the relaxation rate of the low energy electrons ($E_e < 5$ eV), which are responsible for the remaining 6^1P_1 excitation contribution from the 6^3P states, is approximately proportional to the discharge current (i.e. electron density). This relaxation is due to both Coulomb relaxation with the subsequent energy loss suffered at high electron energies, and to relaxation by inelastic collisions with the excited 6^3P density. It can be estimated from Spi 56, Lig 80, Koe 62, Ver 61, Pen 74 and appendix III that at low currents ($n_e = 10^{15} \text{ m}^{-3}$) this relaxation rate is much smaller than the radiative decay rate β , at intermediate currents ($n_e = 10^{16} \text{ m}^{-3}$) it is of the same order, and at high currents the 6^1P_1 excitation has relaxed already within a few μs . As a consequence, at intermediate currents the remaining two-step 6^1P_1 excitation cannot be described anymore by a single exponentially decaying function of time over a period of 5 to 10 times β^{-1} , as is needed for a correct determination of this background excitation. If we still evaluate the measured 6^1P_1 density decay curves with a sum of two exponentials we then obtain for the fast decay rate the artificial behaviour shown in fig. 5.8.

At high currents, after the initial fast accommodation to the situation with zero electric field, the electron energy distribution varies slowly because of the strong coupling with the slowly decaying 6^3P density energy reservoir (Pol 72). The 6^1P_1 density decay curves can be described with a two-exponential sum function again. The data shown in fig. 5.8 were obtained after

making small corrections for the electron impact deexcitation of the 6^1P_1 population as well as for the radial depletion of the mercury ground state density. The first correction, estimated from Ver 61, Koe 62, Pol 72 and chapter III, increases linearly with the current I up to 5-10% at $I = 1$ A (5% for the data in fig. 5-8). The second correction, estimated from Ken 51 and Ver 61, was also proportional to the current and increased with decreasing mercury density up to about 10% at the lowest density for both argon pressures of 33 and 67 Pa. Due to these corrections the uncertainty in β obtained at high currents is about 10%. For those n_{Hg} , where β was determined at low currents with the same accuracy, the 'low current' and 'high current' values of β agree within $\sim 10\%$.

With increasing mercury density the data obtained at low currents become inaccurate due to a decreasing 6^1P_1 density with increasing n_{Hg} , as was observed also for zero noble gas pressure. For these conditions the 'high current' β values were used. The differences between the values at the axis and at the wall of both the temperature and the mercury ground state density are on the average 2% (max. 4%) and 4% (max. 15%), respectively, for these conditions (estimated from Ken 51 and Ver 61). Therefore, we feel that these experimental radiative decay rates can be compared well with those

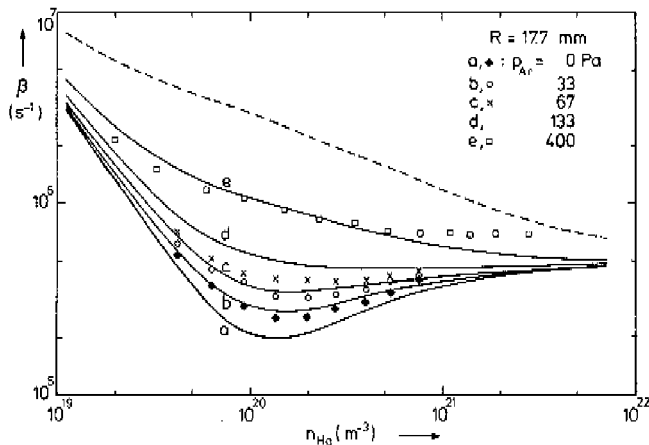


Fig. 5-9 The fundamental mode radiative decay rate β of the Hg 184.9 nm line as a function of the Hg number density n_{Hg} for various Hg-Ar gas mixtures. The data points were obtained using both experimental methods (see text). For $p_{\text{Ar}} = 133$ Pa (curve d) no experimental data were obtained. — : partial frequency redistribution theory of chapter IV; - - - : complete frequency redistribution theory of van Trigt (Tri 76) for $p_{\text{Ar}} = 400$ Pa. Both calculations were made for a natural abundance in the Hg 6^1P_1 population. The data with $p_{\text{Ar}} = 400$ Pa are for $R = 18.0$ mm.

calculated from the theory of chapter IV for a homogeneous medium. The data obtained for the argon pressures $p_{\text{Ar}} = 33 (\pm 3), 67 (\pm 7)$ Pa are shown in fig. 5-9. The accuracy is about 10%.

The β values obtained show a less pronounced minimum in $\beta(n_{\text{Hg}})$ with increasing Ar pressure (see fig. 5-9), which is due to the extra collisional broadening by the Ar gas. For the measurement of β at larger Ar pressures a different experimental technique was used. This technique allowed measurements at low current values – with inherently fewer corrections – and will be described next.

V.2. Laser-induced fluorescence measurements

The laser-induced fluorescence (LIF) measurements were performed in a steady state discharge at low current values. At these currents the steady state density in the 6^3P_2 level is much larger than that in the 6^1P_1 level. Since a significant fraction of the 6^3P_2 density is transferred by the laser pulse to the 6^1P_1 level, the temporary overpopulation in the 6^1P_1 level is larger than the steady state density by a few orders of magnitude. This can also be seen on the 184.9 nm emission intensity. Therefore, any changes in the 184.9 nm steady state emission introduced by the pumping process via a change in $n_{6^1\text{P}}$

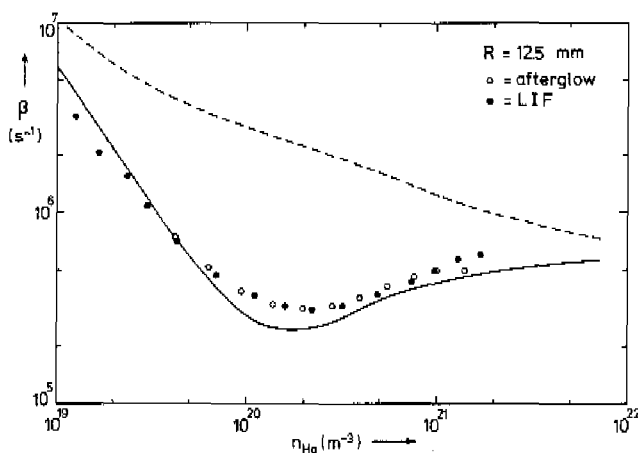


Fig. 5-10 The fundamental mode radiative decay rate β of the Hg 184.9 nm line as a function of the Hg number density n_{Hg} for zero perturber gas pressure as obtained using two different experimental methods (see text). — : partial frequency redistribution theory of chapter IV; - - - : complete frequency redistribution theory of van Trigt (Tri 76). Both calculations were made for a natural abundance in the Hg 6^1P_1 population.

or a change in n_e and T_e via the optogalvanic effect (Wei 85) can be ignored. As a consequence the observed fluorescence can be described with a single exponential decay with rate β above the very low intensity background of the steady state emission.

As a check of the LIF method we first measured b as a function of the mercury density n_{Hg} for $R = 12.5$ mm and zero perturber gas pressure. The β values were obtained in the current region $I = 1-10$ mA, and are independent of I . This confirms our estimate that electron impact processes do not influence the decay rate of the temporary overpopulation in the 6^1P_1 level at these currents. The results are shown in fig 5-10 and are compared with the data obtained with the dye laser absorption measurements. The agreement between the two independent experiments is good. The data agree within the experimental error, which is 5% in both cases, except for the largest n_{Hg} of section V.1, where the result of the afterglow experiment becomes less accurate.

Using the LIF method β can be measured in a larger range of mercury densities than is possible with the afterglow absorption method. At low n_{Hg} values this is because the steady state discharge can be maintained much more easily than the periodically short-circuited discharge. At high n_{Hg} values it is because in the LIF method the overpopulation is created indepen-

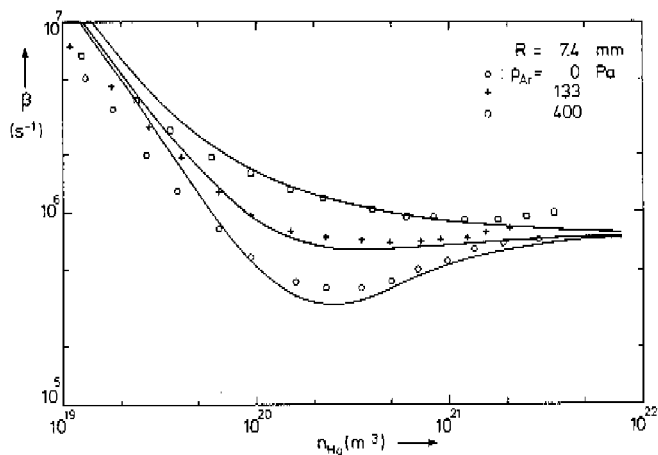


Fig. 5-11 The fundamental mode radiative decay rate β of the Hg 184.9 nm line as a function of the Hg number density n_{Hg} for various Hg-Ar gas mixtures. The experimental data were obtained using the laser-induced fluorescence method. — : theory of chapter IV for a natural abundance in the Hg 6^1P_1 population.

dently of the direct or two-step nature of the excitation in the discharge.

Next $\beta(n_{\text{Hg}})$ was measured with the LIF method for $R = 7.4$ mm as a function of p_{Ar} and for $p_{\text{Ar}} = 400$ Pa as a function of R . The β values were obtained in the low current regions $I = 1$ -10 mA for $p_{\text{Ar}} = 0$ and $I = 0.1$ -1 mA for $p_{\text{Ar}} > 0$, and were again independent of I . The resulting data are shown in figs. 5-9, 5-11 and 5-12. The experimental error is about 5% for $p_{\text{Ar}} = 0$ and about 10% for $p_{\text{Ar}} > 0$, due to the presence of instabilities in the low current discharges, which were more severe in the latter case.

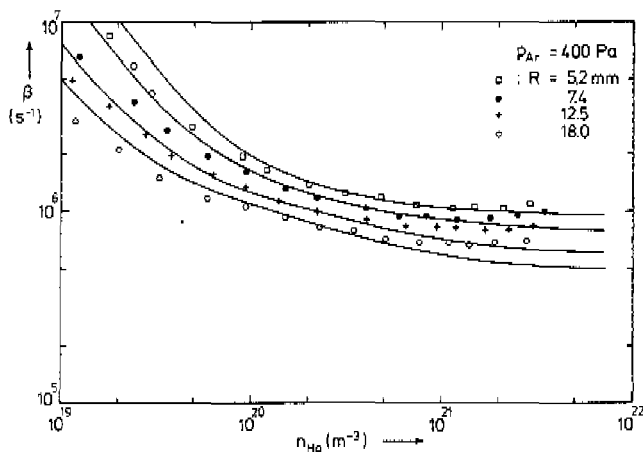


Fig. 5-12 The fundamental mode radiative decay rate β of the Hg 184.9 nm line as a function of the Hg number density n_{Hg} in a Hg-Ar gas mixture for various values of the cylinder radius R . The experimental data were obtained using the laser-induced fluorescence method. —: theory of chapter IV for a natural abundance in the $\text{Hg}6^1\text{P}_1$ population.

The influence upon $\beta(n_{\text{Hg}})$ of an additive background of perturber gas is shown in figs. 5-9 and 5-11. With increasing Ar pressure the minimum in $\beta(n_{\text{Hg}})$ becomes less pronounced until it has disappeared at pressures above ~ 133 Pa. This is due to the extra collisional broadening provided by the argon atoms. The exact pressure value at which the minimum disappears depends slightly upon the value of R , of course (see chapter IV). At an Ar pressure of 400 Pa, $\beta(n_{\text{Hg}})$ is a monotonously decreasing function of n_{Hg} for all R values measured.

We also measured β for $R = 7.4$ mm and 400 Pa of krypton gas pressure. The resulting β values were identical with those for 400 Pa of argon at the same R . This can easily be understood from the theory given in chapter IV,

because the elastic collisional broadening by these two gases is the same: ~ 0.11 MHz/Pa (Bou 77).

In the LIF experiments reported above, the initial radial profile of the created overpopulation was rather similar to that of the 6^3P_2 density in the steady state of the discharge. This was achieved by using for the side-on irradiating laser beam a diameter larger than the discharge diameter. Furthermore the laser beam intensity used was so high that it hardly diminished on passing through the discharge tube because of saturation at the optically thin transition at 365.5 nm. The axial dependence of this overpopulation was determined by the laser beam diameter. The influence of the initial spatial profile of the created overpopulation upon the time dependence of its decay was examined in a separate LIF experiment. In this experiment the overpopulation was created in a narrow cylindrical region, which crossed the discharge cylinder axis perpendicularly. After several microseconds the fluorescence, observed in a direction perpendicular to both cylinder axes, could be described again by a single exponential decay with the same decay rate as with the broader initial radial profile.

V.3. Comparison with theory

We conclude from the above results that in our experimental conditions the fast decay of an initial 6^1P_1 overpopulation, which is governed by radiation transport processes, is described well after some time by a single exponential decay, i.e. a single radiative decay rate. This is in agreement with the theory for this regime, described in chapter IV, from which we calculate that the condition for the existence of a fundamental mode is largely satisfied: $P_c + \eta(\tau_c) > 100 \beta/\gamma$ in all experimental conditions (see chapter IV).

The fundamental mode radiative decay rate β for the 184.9 nm Hg line was calculated with the partial redistribution theory of chapter IV on the assumption of a natural abundance in the 6^1P_1 excited state and is shown in figs. 5-4, 5-5, 5-9-5-12. The contributions β_{nc} and β_c in eq. (4-21) of chapter IV are shown in fig. 5-4. Values of β calculated with the complete redistribution theory (Tri 76) on the same assumption are shown for zero perturber gas pressure (fig. 5-4, 5-10), as well as for 400 Pa of argon as perturber gas (fig. 5-5). These values can be larger than the experimental data by as much as a factor of 8 and 3, respectively. Using the theory of chapter IV the agreement is much better. For $a(x)$ we used the expression in eq. (4-22.).

The escape function η was calculated with the frequency independent radial profile $f_D(\rho)$ for all mercury densities (see section IV.2). For $R = 12.5$ mm and $n_{Hg} < 2 \cdot 10^{20} \text{ m}^{-3}$ $f_D(\rho)$ is a good approximation. For $R = 12.5$ mm

and $n_{\text{Hg}} > 2 \cdot 10^{20} \text{ m}^{-3}$ the influence of the uncertainty in $f(\rho)$ is small: $f(\rho)$ equal to $J_0(2.404\rho)$ or $f_L(\rho)$ leads to 7% higher or 4% lower β values, respectively, whereas the values obtained with $\eta(\tau_c)$ from the analytical expression (4.29) are $< 3\%$ lower. For the other R values the uncertainties are about the same.

The atomic data used for the calculations are the natural lifetime $\tau_n = 1.31 \text{ ns}$ (Lur 65) and the hyperfine structure of the line (Leb 74, Ger 77, Nie 50). The Voigt line profile was calculated using the routine given in Gau 70. The optical thickness at the axis of the cylinder $\tau_x = k(x)R$ is shown in fig. 5-6 for the complete Voigt line as well as the Doppler line profiles of the h.f.s. and $n_{\text{Hg}} = 2 \cdot 10^{20} \text{ m}^{-3}$. This figure also gives a good impression of the situation in the whole range of experimental conditions reported, since a_x increases less than a factor of 2 with respect to the value used in fig. 5-6.

For the Hg collisional broadening we used the theory of Ber 69 and Omo 68 for resonant collisions. In our case, where the hyperfine interaction is not small enough to be neglected during the collision (see Omo 68), this theory applies only for the even isotopes, which have zero nuclear spin. These represent 70% of the total mercury density in the natural abundance (Nie 50). We assumed that the broadening for the h.f. levels of the odd Hg isotopes, which have non-zero nuclear spin, is equal to that for the even ones. Using eq. (4.3) with $\zeta = 1$, we find for P_c from eq. (4.5b):

$$P_c = \frac{0.029 n_{\text{Hg}}}{1 + 0.029 n_{\text{Hg}}}, \quad n_{\text{Hg}} \text{ in } 10^{20} \text{ m}^{-3}.$$

The use of the theory of Gay 74 for quasi-resonant collisions, which also applies for the even isotopes only, would yield an averaged 15% lower collision rate for the total h.f.s. ($\zeta = 0.85$ in eq. (4.3)), on the same assumption as used above. This would have resulted in values of the decay rate β which, for mercury densities of $4 \cdot 10^{19}$, $2 \cdot 10^{20}$ and $1 \cdot 10^{21} \text{ m}^{-3}$, are only 1, 13 and 11 percent lower than those obtained with $\zeta = 1$. For the broadening by Ar as collision partner we used the experimental data of Bou 77. The line shift induced in these Hg-Ar collisions was neglected, because it is less than 1% of the Doppler width for all experimental conditions (Bou 77).

We will next discuss the comparison between the theoretical and experimental decay rates in more detail. We start with zero perturber gas pressure and low mercury densities. It is seen from figs. 5-5, 5-10, 5-11 that the theoretical decay rate, calculated for a natural abundance in the excited 6^1P_1 population, is larger than the experimental one at mercury densities less than a critical value $n_1(R)$, which is given by $n_1(R) \approx 5 \cdot 10^{17}/R \text{ m}^{-3}$ (R in m). At

the lowest mercury densities the difference can be as large as a factor of two. In this regime, where the radiation transport is dominated by the Doppler redistribution mechanism in the line core (see chapter IV), the theory is supposed to be good, and this discrepancy is unexpected at first sight. We will next show that this is most likely caused by a deviation from natural abundance in the excited 6^1P_1 state population, due to the particular h.f.s. of the 184.9 nm line. The density $n_1(R)$ corresponds to an optical thickness $k(x_{\min})R \approx 3$ in the minimum of $k(x)R$ between the ^{204}Hg component and the other mutually overlapping components of the 184.9 nm h.f.s. (see fig. 5-6). The quantity x denotes the reduced photon frequency distance to the line centre (see chapter IV); x_{\min} is the value at the minimum in $k(x)R$. For mercury densities less than $n_1(R)/3$, e.g. $n_{\text{Hg}} = 1 \cdot 10^{19} \text{ m}^{-3}$ and $R < 17 \text{ mm}$, we find that $k(x_{\min})R < 1$. Therefore, at these optical thicknesses the ^{204}Hg isotope has only a weak radiative coupling to the other isotopes. It can be shown, using the collision rates given in Ber 69 and Gay 74, that also the coupling via resonant collisions, which transfer the excited state energy, is small. Furthermore, the ^{204}Hg component itself has a 12 times larger decay rate than the other strongly coupled line components, because of its 12 times smaller optical thickness. As a consequence, after a very short time the ^{204}Hg component also decays with the 'slow' radiative decay rate of the strongly coupled components. Further, the population in the ^{204}Hg 6^1P_1 level, determined by the coupling and radiative decay rates, is much less than according to the natural abundance. Because the ^{204}Hg component contributes about 50% of the escaping photon fraction in a natural abundance distribution, it follows that this underpopulation can result in a 50% lower decay rate than calculated for a natural abundance distribution in the 6^1P_1 population.

This deviation from natural abundance gradually decreases with increasing n_{Hg} , in our conditions mainly due to an increasing radiative coupling of the h.f.s. components. An exact calculation of this coupling has to take account of the correct frequency redistribution of the coherently scattered photons in the wings of the h.f.s. line components, which is not done here. It should be remarked that the experiments presented here provide interesting test material for such calculations. A sufficiently accurate experimental determination of the relative ^{204}Hg 6^1P_1 population was not possible with our set-up. For this purpose Doppler free techniques can best be used. This is because in the transitions to higher levels the lines for the even isotopes strongly overlap each other and because furthermore the ^{204}Hg isotope constitutes about 10% of the total even isotopes.

For mercury densities larger than n_1 , we have for the optical thickness at x_{\min} : $k(x_{\min})R > 3$, and photons emitted at x_{\min} undergo many scattering

events before they can escape from the volume at this frequency. Because of the frequency redistribution over a frequency interval $\Delta x_1 = 0.7$ per scattering event (Ost 62; see also appendix IV.C), it can be assumed that the radiative coupling at these optical thicknesses is sufficiently strong to maintain a natural abundance distribution to a good approximation. For $n_{\text{Hg}} > n_1(R)$ and zero perturber gas pressure we find that $\beta_{\text{th}} < \beta_{\text{exp}}$. This is probably due to an approximation made in the theory of chapter IV ($\Delta x_1 \rightarrow 0$ in the line wings), which neglects diffusion in frequency space of photons in the line wings to optically thinner regions; see appendix IV.C.

With the addition of perturber gas as an extra (decorrelating) collision partner, the overestimation by the theory at low mercury densities remains, because the created extra radiative coupling between the line components is too small at these pressures. For medium mercury densities the underestimation by the theory near the minimum in $\beta(n_{\text{Hg}})$ becomes less with increasing perturber gas pressure, because the error introduced by the above-mentioned approximation in the theory becomes smaller. At the largest mercury densities measured the difference between β_{th} and β_{exp} increases with increasing Ar pressure. This may be due to the deviation of the (emission and absorption) line profile from a Voigt line profile in the far wings of the 184.9 nm line, which was found for Ar and Kr as collision partners (Bra 79). This deviation is about equal for Ar and Kr gas, which, together with the already mentioned equal collision broadening, explains the equal β_{exp} values found for the mercury noble-gas mixtures with 400 Pa of Ar or Kr (see section V.2). Measurements with He as a perturber gas would be interesting in this respect, since for this gas the 184.9 nm line profile is a Voigt line profile in a much wider spectral region (Bra 79).

We conclude that when corrections are made for the deviation from natural abundance in the 6^1P_1 excited state population at the lowest mercury densities, the agreement between the experiments and the theory of chapter IV is within 25% for all experimental conditions reported.

REFERENCES

- Ber 69 P. R. Berman and W. E. Lamb, *Phys. Rev.* **187**, 221 (1969).
 Bou 77 C. Bousquet and N. Bras, *J. Phys.* **38**, 139 (1977).
 Bra 79 N. Bras and C. Bousquet, *J. Phys.* **40**, 945 (1979).
 Gau 70 W. Gautschi, *S.I.A.M. J. Num. Anal.* **7**, 187 (1970).
 Gay 74 J. C. Gay, *J. Phys.* **35**, 813 (1974).
 Gem 75 M. I. C. van Gemert, *J. Appl. Phys.* **46**, 4899 (1975).
 Ger 77 S. Gerstenkorn, J. J. Labarthe and J. Vergès, *Physica Scripta* **15**, 167 (1977).
 Kag 68 Yu. M. Kagan and B. Kasmaliév, *Opt. Spectr.* **24**, 356 (1968).
 Ken 45 C. Kenty and J.R. Cooper, *Trans. Electrochem. Soc.* **87**, 397 (1945).
 Ken 51 C. Kenty, M. A. Easley and B. T. Barnes, *J. Appl. Phys.* **22**, 1006 (1951).
 Kla 38 B. Klarfeld, *Tech. Phys. USSR* **5**, 913 (1938).
 Kle 21 O. Klein and S. Rosseland, *Z.f. Physik* **4**, 46 (1921).
 Koe 62 M. Koedam and A. A. Kruihof, *Physica* **28**, 80 (1962).
 Lab 71 P. Laborie, J.-M. Rocard and J. A. Rees, 'Electronic cross sections and macroscopic coefficients' Vol. 2, Dunod, Paris (1971).
 Leb 74 E. Lehoucher, C. Bousquet and N. Bras, *Nouv. Rev. Optique* **5**, 121 (1974).
 Note that the energy value of the 201-1/2 component in MHz units has been misprinted. The correct value should be 8720 MHz. The energy value of the ¹⁹⁹Hg component was obtained using Ger 77.
 Lig 80 F. A. S. Lighthart and R. A. J. Keijser, *J. Appl. Phys.* **51**, 5295 (1980).
 Lur 65 A. Lurio, *Phys. Rev.* **140A**, 1505 (1965).
 Mas 71 H. S. W. Massey, 'Electronic and ionic impact phenomena' Vol. 3, Chapter 8, Clarendon Press, Oxford (1971).
 Mur 50 K. Murakawa and S. Suwa, *J. Phys. Soc. Jap.* **5**, 429 (1950).
 Nie 50 A. O. Nier, *Phys. Rev.* **79**, 450 (1950).
 Omo 68 A. Omont and J. Meunier, *Phys. Rev.* **169**, 92 (1968).
 Ost 62 D. E. Osterbrock, *Astrophys. J.* **135**, 195 (1962).
 Pay 74 M. G. Payne, J. E. Talmage, G. S. Hurst and E. B. Wagner, *Phys. Rev.* **A9**, 1050 (1974).
 Pen 74 N. P. Penkin and T. P. Redko, *Opt. Spectr.* **36**, 258 (1974).
 Phe 59 A. V. Phelps, *Phys. Rev.* **114**, 1011 (1959).
 Pol 72 J. Polman, *J. Appl. Phys.* **43**, 1577 (1972).
 Sac 82 H. T. Saelce, *J. Phys.* **D15**, 873 (1982).
 Sem 77 I. V. Semenova and Yu. M. Smirnov, *Opt. Spectr.* **42**, 477 (1977).
 Spi 56 L. Spitzer, Jr., 'Physics of fully ionized gases', Interscience, New York (1956), ch.5.
 Tri 76 C. van Trigt, *Phys. Rev.* **A13**, 726 (1976).
 Ver 61 W. Verweij, *Philips Res. Rep. Suppl.* **2** (1961).
 Wei 82 P. van de Weijer and R. M. M. Cremers, *J. Appl. Phys.* **53**, 1401 (1982).
 Wei 85 P. van de Weijer and R. M. M. Cremers, *Opt. Comm.* **53**, 109 (1985).

VI. Concluding Remarks

- The absolute scale of the Hg 6^1P_1 direct electron impact excitation cross section can be determined in a low-pressure mercury discharge with reasonable accuracy ($\sim 30\%$) when the discharge conditions are suitably chosen.

The cascade contribution to the total 6^1P_1 excitation cross section, i.e. including cascade excitation, is less than about 15% for electron energies below 15 eV. Apparently therefore the most recent experimental 6^1P_1 excitation cross section in literature (1962) is much too small.

The present value is a factor of two lower than the one other experimental value dating from 1935, and about a factor of three lower than theoretical results.

- For the fundamental mode radiative decay rate β of a system of excited atoms an analytical expression can be obtained from a theory of partial redistribution in frequency.

The expression for the decay rate can be derived for a hyperfine structure of the line with a natural abundance distribution in the excited state population and applies for a homogeneous medium at large optical thickness and a wide range of collision rate values.

A condition can be derived for the existence of a fundamental mode. In the experiments performed on the decay rate of the 6^1P_1 population this condition was largely satisfied.

The analytical expression for the decay rate consists of an integral over the photon frequency of the emission line profile weighted with an escape function.

An approximation can be made in this escape function which considerably simplifies the calculation of the decay rate at the expense of only a small error.

- The Hg 6^1P_1 density decay curves obtained in the afterglow of a low-pressure mercury noble-gas discharge can be used to measure the radiative decay rate of the 6^1P_1 population.

Radiative decay rate values obtained from the Hg 6^1P_1 density decay curves in the afterglow of a low-pressure mercury discharge and values obtained from the laser-induced fluorescence at the 184.9 nm line created by pulsed optical pumping in a steady state discharge are in good agreement with each other.

The radiative decay rate as a function of the mercury density $\beta(n_{\text{Hg}})$ shows

a pronounced minimum in the case of zero perturber gas density. The presence of a minimum in $\beta(n_{\text{Hg}})$ in a density range where the Voigt absorption line profile varies only slightly, clearly shows that β is not a function of the optical thickness at line centre and of the absorption line profile only, in marked contrast with the complete redistribution formulation.

The minimum in the decay rate β as a function of n_{Hg} is caused by a decreasing contribution from the Doppler redistribution mechanism with increasing mercury density, in combination with an increasing contribution from the collisional redistribution mechanism.

The minimum in $\beta(n_{\text{Hg}})$ is less pronounced for mercury noble-gas mixtures due to the constant extra collisional broadening provided by the noble gas atoms.

The minimum in $\beta(n_{\text{Hg}})$ for our tube radii of 6-18 mm is absent for mercury-argon gas mixtures with more than about 15 MHz extra collisional broadening due to the Ar atoms, i.e. mixtures with argon densities larger than about $3 \cdot 10^{22} \text{ m}^{-3}$.

The experimental decay rates at the lowest mercury densities are smaller than the theoretical ones calculated for a natural abundance in the excited 6^1P_1 population. This could be interpreted as due to a deviation from the natural abundance in the $^{204}\text{Hg } 6^1\text{P}_1$ population.

The deviation from natural abundance in the $^{204}\text{Hg } 6^1\text{P}_1$ population could provide interesting information about the radiative coupling of the ^{204}Hg component of the 184.9 nm hyperfine structure to the mutually overlapping h.f.s. components of the other isotopes. The experimental determination could be performed best with Doppler free techniques.

The experimental radiative decay rates can be up to a factor of 8 lower than those calculated from the usual complete redistribution theory. The agreement with radiative decay rates calculated from our partial redistribution theory is within about 25%.

Summary

The low-pressure mercury noble-gas discharge is of great practical interest because of its application in fluorescent lamps (TL*, SL*, PL*). The Hg resonance radiation at the 253.7 nm and 184.9 nm UV lines originating from the levels 6^3P_1 and 6^1P_1 respectively is mainly responsible for the light production in fluorescent lamps. The contribution of the 184.9 nm line to the total UV production can amount to $\sim 30\%$.

The subject of this thesis is a quantitative study of the main processes responsible for the UV output at the 184.9 nm line of low-pressure mercury noble-gas discharges. These processes are

1. excitation of the 6^1P_1 level by electron impact from the 6^1S_0 ground state as well as from the nearby 6^3P states.
2. radiative decay of the 6^1P_1 population under the influence of strong radiation trapping at the 184.9 nm resonance line. Due to this process the escape rate of the resonance photons from the volume can be several orders of magnitude lower than the natural decay rate of the dipole transition.

For both processes no sufficiently reliable quantitative data nor theoretical expressions to calculate them from were available in the literature. However, such data are essential if we want to calculate the radiated power at the 184.9 nm line from the microscopic discharge parameters, as is frequently done in model calculations. We studied these processes quantitatively from both the experimental and the theoretical point of view.

In the following we will summarize our study of the processes under 1. and 2.

1. Hg 6^1P_1 excitation cross sections

We have determined the absolute scale of the Hg 6^1P_1 direct electron impact excitation cross section in the positive column of a low-pressure mercury discharge. This was done in a regime where the electron impact excitation of the investigated Hg levels is predominantly from the ground state, and radiative decay is the dominant depopulation mechanism. The tube radius is 12.5 mm, the mercury density $4 \cdot 10^{19} - 2 \cdot 10^{20} \text{ m}^{-3}$ and the discharge current 10 - 100 mA. The radiative decay rate of the Hg 6^1P_1 level was determined using dye laser absorption measurements of the 6^1P_1 density in the steady state and in the afterglow of the discharge. From these data we

deduced the excitation rate of the 6^1P_1 level. The electron density and temperature in the tail of the energy distribution were obtained from measurements of the radiances at optically thin lines with known excitation function. Using the shape of the optical excitation function of the 184.9 nm line from the literature we obtained its absolute scale from our experimental data. The cascade contribution to this total cross section was less than 15% for $6.7 \leq E_e \leq 15$ eV. Apparently the most recent experimental value in literature (1962) is much too small. The initial slope of the 6^1P_1 direct excitation cross section is $(0.35 \pm 0.1) 10^{-20} \text{ m}^2/\text{eV}$, the cross section at 15 eV is $(2.1 \pm 0.6) 10^{-20} \text{ m}^2$. This value is a factor of 2 lower than the one other experimental value dating from 1935 and about a factor of 3 lower than theoretical results.

Using our absolute cross section for excitation of the 6^1P_1 level from the ground state, we also estimated the cross section for its excitation from the 6^3P states. The initial slope of this cross section is $1.4 10^{-20} \text{ m}^2/\text{eV}$. For this estimate we used the extensive experimental data available in literature for the low-pressure mercury-argon discharge with a tube radius of 18 mm and an argon pressure of 400 Pa.

2. Radiative decay rate

Measurements were made of the fundamental mode radiative decay rate of the Hg 6^1P_1 population over a wide range of experimental conditions in a cylindrical geometry. In this range strong radiation trapping occurs at the 184.9 nm resonance line along with low collision rates. The measurements were performed using two different experimental methods, both employing low-pressure mercury noble-gas discharges. In the first method the decay rate of the 6^1P_1 population was measured in the afterglow of the discharge using a dye laser absorption technique. In the second one the decay was measured of the laser-induced fluorescence at the 184.9 nm line created by pulsed optical pumping. Radiative decay rates obtained with the two independent experimental methods for nominally the same conditions agreed within the experimental error of 5%.

For zero noble gas density the radiative decay rate β as a function of the mercury density n_{Hg} shows a pronounced minimum. For the tube radius of 12.5 mm as an example, the minimum in β/γ occurs at the mercury density of $\sim 2 10^{20} \text{ m}^{-3}$ and amounts to $4 10^{-4}$. This minimum in $\beta(n_{\text{Hg}})$ disappears with the addition of an argon density of more than about $3 10^{22} \text{ m}^{-3}$, which corresponds to an extra collisional broadening of more than about 15 MHz.

The experimental rates can be up to a factor of 8 lower than those calculated from theory with the usual assumption of complete redistribution. Indeed, complete redistribution is not expected in the present case, where the optical thickness is large and the elastic collision rate γ_c is smaller than the single atom spontaneous emission rate γ .

We derived an analytical expression for the fundamental mode radiative decay rate from a theory based on partial redistribution in frequency. The expression is valid for a homogeneous medium at large optical thickness in a wide range of γ_c/γ values and applies also for a hyperfine structure of the resonance line. A condition is given for the existence of a fundamental mode and is shown to be largely satisfied in our experiments. The radiative decay rates calculated with this expression agree with our experimental rates within 25%. The behaviour of the experimental rates at the lowest mercury densities could be interpreted as due to a deviation from the natural abundance in the 6^1P_1 excited state population.

Samenvatting

De lage-druk kwik-edelgasontlading is van groot praktisch belang door zijn toepassing in fluorescentielampen (TL*, SL*, PL*). De resonantie straling van kwik op de 253.7 nm en 184.9 nm-UV-lijnen, welke afkomstig zijn van respectievelijk de 6^3P_1 en 6^1P_1 -niveaus is voornamelijk verantwoordelijk voor de lichtproductie in fluorescentielampen. De bijdrage van de 184.9 nm-lijn aan de totale productie van ultraviolet licht kan oplopen tot ~30%.

Dit proefschrift bevat een kwantitatieve studie van de voornaamste processen die verantwoordelijk zijn voor de UV-opbrengst op de 184.9 nm-resonantielijns van Hg (6^1S_0 - 6^1P_1) in lage-druk kwik-edelgasontladingen. Deze processen zijn:

1. aanslag van het 6^1P_1 -niveau door elektronenbotsingen vanuit zowel de 6^1S_0 -grondtoestand als de nabijgelegen 6^3P -toestanden.
2. stralend verval van de 6^1P_1 -bevolking onder invloed van sterke stralingsinvangst op de 184.9 nm-resonantielijns. Als gevolg van dit proces kan de ontsnappingssnelheid van de resonantiefotonen uit het volume enkele grootte-orden kleiner zijn dan de spontane emissiesnelheid van een enkel atoom.

Voor beide processen waren geen voldoende betrouwbare kwantitatieve gegevens beschikbaar in de literatuur, noch theoretische uitdrukkingen om deze te kunnen berekenen. Echter, zulke gegevens zijn van wezenlijk belang als we het uitgestraalde vermogen op de 184.9 nm-lijn willen berekenen uit de microscopische ontladingsparameters, zoals vaak gedaan wordt bij modelberekeningen. We hebben deze processen kwantitatief bestudeerd zowel op experimentele wijze als vanuit een theoretische ooghoek.

We zullen nu eerst onze studie van de processen onder punt 1 bespreken en daarna die met betrekking tot punt 2.

1. Botsingsaanslag van het Hg 6^1P_1 -niveau

We hebben de absolute grootte bepaald van de werkzame doorsnede voor de elektronenbotsingsaanslag van het Hg 6^1P_1 -niveau in een lage-druk kwik-ontlading. Dit werd gedaan in een ontladingsregime waar de elektronen botsingsaanslag van de onderzochte Hg-niveaus voornamelijk vanuit de grondtoestand plaatsvindt, en waar verder stralend verval het voornaamste ontvolkingsmechanisme is. De buisstraal is 12.5 mm, de kwikdichtheid

$4 \cdot 10^{19} - 2 \cdot 10^{20} \text{ m}^{-3}$ en de ontladingsstroom $10 - 100 \text{ mA}$. De stralende vervalsnelheid van het $\text{Hg } 6^1\text{P}_1$ -niveau werd bepaald uit metingen van de 6^1P_1 -dichtheid met een absorptie-methode, waarbij een kleurstof-laser als lichtbron gebruikt werd. De metingen werden gedaan in zowel de stationaire ontlading als de nagloei van de ontlading wanneer deze snel werd uitgeschakeld. Uit deze gegevens leidden we de aanslagsnelheid van het 6^1P_1 -niveau af. De elektronendichtheid en de -temperatuur in de staart van de energie-verdeling werden verkregen uit metingen van de luminantie op optisch dunne emissielijnen met een bekende aanslagfunctie. Uit de experimentele gegevens verkregen we de absolute waarde van de optische aanslagfunctie van de 184.9 nm -lijn voor de aanslag door elektronenbotsingen. Hierbij gebruikten wij de vorm van de functie uit de literatuur. De cascadebijdrage aan deze totale werkzame doorsnede was minder dan 15% voor $6.7 \leq E_e \leq 15 \text{ eV}$. Klaarblijkelijk is de meest recente experimentele waarde uit de literatuur (1962) veel te klein. De helling van de werkzame doorsnede voor de directe aanslag van het 6^1P_1 -niveau vlak boven de drempel is $(0.35 \pm 0.1) \cdot 10^{-20} \text{ m}^2/\text{eV}$, de werkzame doorsnede bij 15 eV is $(2.1 \pm 0.6) \cdot 10^{-20} \text{ m}^2$. Deze waarde is een faktor twee lager dan de enige andere experimentele waarde, daterend uit 1935, en ongeveer een faktor drie lager dan theoretisch gevonden waarden.

Gebruik makend van onze absolute werkzame doorsnede voor aanslag van het 6^1P_1 -niveau vanuit de grondtoestand, konden wij tevens een schatting maken van de werkzame doorsnede voor de aanslag van het 6^1P_1 -niveau vanuit de 6^3P -toestanden. De helling van deze werkzame doorsnede vlak boven de drempel is $1.4 \cdot 10^{-20} \text{ m}^2/\text{eV}$. Hiervoor gebruikten we de uitgebreide reeks van experimentele gegevens die in de literatuur beschikbaar is voor de lage-druk kwik-argon-ontlading met een buisstraal van 18 mm en een argon-druk van 400 Pa .

2. Stralende vervalsnelheid

De stralende vervalsnelheid in de fundamentele mode van de $\text{Hg } 6^1\text{P}_1$ -bevolking is gemeten over een breed gebied van experimentele omstandigheden in een cilindrische geometrie. In dit gebied heerst sterke stralings-invangst op de 184.9 nm -resonantielij, gepaard gaande met een lage botsingssnelheid. De metingen werden gedaan met twee verschillende experimentele methoden, die beide gebruik maakten van lage-druk kwik-edelgasontladingen. Bij de eerste methode werd de vervalsnelheid van de 6^1P_1 -bevolking gemeten in de nagloei van de ontlading met een absorptie-techniek

waarbij een kleurstof-laser als lichtbron gebruikt werd. Bij de tweede methode werd het verval gemeten van de door een laser geïnduceerde fluorescentie op de 184.9 nm-lijn, welke werd gecreëerd door gepulseerd optisch pompen. Stralende vervalsnelheden verkregen met de twee onafhankelijke experimentele methoden voor nominaal dezelfde omstandigheden kwamen met elkaar overeen binnen de experimentele fout van 5%.

Voor omstandigheden zonder edelgas vertoont de stralende vervalsnelheid β als functie van de kwikdichtheid n_{Hg} een uitgesproken minimum. Voor de buisstraal van 12.5 mm als voorbeeld, treedt het minimum in β/γ op bij de kwikdichtheid van $\sim 2 \cdot 10^{20} \text{ m}^{-3}$ en heeft de waarde $4 \cdot 10^{-4}$. Dit minimum in $\beta(n_{\text{Hg}})$ verdwijnt met de toevoeging van argondichtheden groter dan ongeveer $3 \cdot 10^{22} \text{ m}^{-3}$, wat overeenkomt met een extra botsingsverbreding van meer dan ongeveer 15 MHz. De experimentele vervalsnelheden kunnen tot een factor 8 kleiner zijn dan die berekend met de gebruikelijke complete redistributie theorie. Inderdaad wordt ook geen volledige herverdeling van de frequentie verwacht in het onderhavige geval, waar de optische dichtheid groot is en de elastische botsingssnelheid γ_c kleiner is dan de spontane emissiesnelheid γ van een enkel atoom.

We hebben een analytische uitdrukking afgeleid voor de stralende vervalsnelheid in de fundamentele mode met een theorie die gebaseerd is op gedeeltelijke herverdeling van de frequentie. De uitdrukking is geldig voor een homogeen medium bij grote optische dichtheid in een groot bereik van de verhouding γ_c/γ , en geldt tevens voor een hyperfijnstructuur van de resonantielijnen. Een voorwaarde wordt gegeven voor het bestaan van een fundamentele mode en we laten zien dat hieraan ruimschoots voldaan is in onze experimentele omstandigheden. De stralende vervalsnelheden, berekend met deze uitdrukking, komen met de experimenteel gevonden waarden overeen binnen 25%. Het gedrag van de experimentele vervalsnelheden bij de laagst gemeten kwikdichtheden kon geïnterpreteerd worden als het gevolg van een afwijking van de natuurlijk voorkomende verdeling in de bevolking van het aangeslagen 6^1P_1 -niveau.

Dankwoord

Het onderzoek beschreven in dit proefschrift is verricht in het Natuurkundig Laboratorium van de N.V. Philips' Gloeilampenfabrieken te Eindhoven. De directie van dit laboratorium ben ik erkentelijk voor hun toestemming de resultaten van dit onderzoek te publiceren in deze vorm.

Graag wil ik iedereen bedanken die op een of andere wijze aan het tot stand komen van dit proefschrift heeft bijgedragen.

In het bijzonder dank ik Dr. Q.H.F. Vreken voor de vele verdiepende discussies. Deze hebben zeer bijgedragen tot mijn vorming als fysicus. Bovendien voorzag hij mijn manuscripten met gulle hand van waardevolle suggesties.

Aan alle leden van de gasontladingsgroep denk ik gaarne terug vanwege de collegiale sfeer. Van Peter van de Weijer leerde ik dat twee meer kunnen dan één. Voor de gasontladingsbuizen kon ik steeds terecht bij de mannen van de glastechnische afdeling onder leiding van Michel van Weert. De tekeningen werden met zorg vervaardigd door de grafische ontwerpgroep en door Rob Cremers. Karin Vrijzen en Karin van Kemenade-Serier verzorgden snel en accuraat het vele typewerk.

Ems, jou dank ik voor je steun en opofferingsgezindheid. Deze waren onontbeerlijk voor het slagen van dit project.

Curriculum Vitae

De schrijver van dit proefschrift werd op 11 mei 1951 te Nijmegen geboren. In 1969 behaalde hij het diploma Gymnasium- β aan het Nijmeegs Lyceum. In datzelfde jaar begon hij met zijn studie wis- en natuurkunde aan de Rijksuniversiteit te Groningen. Na in 1972 het kandidaatsexamen (N2) te hebben afgelegd, behaalde hij op 14 december 1976 het doctoraal diploma natuurkunde in de gemengde experimentele en theoretische richting met bijvak wiskunde. Beide doctoraalonderzoeken werden verricht in Utrecht. Het experimentele werk werd gedaan aan het FOM Instituut voor Plasmafysica te Jutphaas; het theoretische onderzoek bij de vakgroep 'Vaste Stof' van de Rijksuniversiteit te Utrecht.

Op 1 januari 1977 trad hij in dienst van de N.V. Philips' Gloeilampenfabrieken als wetenschappelijk medewerker van het Natuurkundig Laboratorium te Eindhoven. Tot 1 oktober 1978 werkte hij in de groep 'Magnetische Registratie', daarna in de groep 'Gasontladingen'. De resultaten van zijn werk in deze laatste groep onder leiding van Dr. Q.H.F. Vreken zijn vastgelegd in dit proefschrift.

Sinds 1 februari 1985 is hij werkzaam bij de Hoofd Industrie-Groep Elcoma van Philips, in de groep 'Passieve Componenten'.

STELLINGEN

behorende bij het proefschrift

**EXCITATION AND RADIATIVE DECAY OF THE
184.9 nm Hg RESONANCE LINE IN
LOW-PRESSURE MERCURY NOBLE-GAS DISCHARGES**

door

H.A. Post

18 oktober 1985

I

Jongorius¹ neemt ten onrechte aan dat de optische aanslagfunctie van de 184.9 nm kwik-lijn voor botsingsaanslag door elektronen met energie beneden 12 eV volledig bepaald wordt door de cascadebijdrage. De door hem gegeven absolute waarde van de aanslagfunctie is daardoor veel te klein.

¹ H. M. Jongorius, Philips Res. Rep. Suppl. 2 (1962).
Dit proefschrift, hoofdstuk III.

II

In kwik van het natuurlijke isotopenmengsel kan bij excitatie een flinke onderbezetting optreden van de aangeslagen 6^1P_1 -toestand in het ^{204}Hg -isotoop.

Dit proefschrift, hoofdstuk V.

III

Het gebruik van de door Jefferies en White¹ ingevoerde benadering in de foton-redistributiefunctie levert in een beperkt dichtheidsgebied een onderschatting van de stralende vervalsnelheid op. In het geval van een minimum in de vervalsnelheid als functie van de dichtheid wordt dan een te geprononceerd minimum berekend.

¹ J. Jefferies and O. White, *Astrophys. J.* **132**, 767 (1960).
Dit proefschrift, hoofdstukken IV, V.

IV

Bij hoge kwikdichtheden is een Voigt-lijnvorm geschikter om de stralingsredistributiefunctie van de 184.9 nm-kwiklijn te beschrijven voor een Hg-He-gasmengsel dan voor een Hg-Ar- of een Hg-Kr-gasmengsel.

Dit proefschrift, hoofdstuk V.

V

Ingold¹ geeft een schatting van de invloed van Ar-Hg Penning-ionisatie op de ionisatiebalans van een lage-druk kwik-argonontlading. Daarbij verwaarloost hij ten onrechte afwijkingen van een Maxwell'se elektronen-energieverdeling voor hoge elektronen-energieën^{2,3}. Dit leidt tot een overschatting van het belang van het genoemde ionisatiemechanisme.

¹ J. H. Ingold in 'Gaseous Electronics' Vol. I, eds. M. N. Hirsch and H. J. Oskam, Acad. Press, New York, 1978.

² N. A. Vorob'eva, Yu. M. Kagan and V. M. Milenia, *Sov. Phys. Tech. Phys.* **9**, 632 (1964).

³ F. A. S. Ligthart and R. A. J. Keijser, *J. Appl. Phys.* **51**, 5295 (1980).

VI

Het gebruik van een mengsel van kwik-isotopen met een sterk verhoogde fractie van het ^{196}Hg -isotoop leidt bij de 253.7 nm-lijn tot een verhoging van de stralende vervalsnelheid¹. Zo'n verhoging treedt niet op bij de 184.9 nm-lijn. Deze kan voor niet al te hoge kwikdichtheid wel verkregen worden door verhoging van de fractie van het ^{204}Hg -isotoop.

¹ M. W. Grossman, S. G. Johnson and J. Maya, *J. Illum. Eng. Soc.* 13, 89 ('83).

VII

Metingen van Shpenik et al.¹ tonen aan dat de vorm van de werkzame doorsnede voor elektron-botsingsaanslag van het 6^3P_2 -niveau van kwik vlak boven de aanslagdrempel verschilt van de door Borst² aangenomen vorm. Dit maakt de absolute waarde van de werkzame doorsnede, zoals bepaald door Borst, onzeker.

¹ O. B. Shpenik et al., *Sov. Phys. - JETP* 42, 23 (1976).

² W. L. Borst, *Phys. Rev.* 181, 257 (1969).

VIII

Het kwikatoom heeft een aantal autoioniserende toestanden van de $5d^96s^26p$ -configuratie in het energiegebied van een paar eV boven de ion-grondtoestand¹. Voor een beter kwantitatief begrip van een lage-druk kwik-edelgasontlading dient de invloed onderzocht te worden van deze niveaus zowel op de werkzame doorsnede voor elektron-botsingsionisatie van de 6^3P -niveaus, als op de werkzame doorsnede voor impulsuitwisseling bij botsingen van elektronen met Hg^+ -ionen in de grondtoestand.

¹ W. C. Martin, J. Sugar and J. L. Tech, *Phys Rev.* A6, 2022 (1972).

IX

In zijn berekening van de scalaire polariseerbaarheid van de 6^1S_0 -grondtoestand van het Hg-atoom houdt Standage¹ ten onrechte geen rekening met bijdragen van niveaus van de $5d^96s^26p$ -configuratie². Dit geeft een onderschatting met ongeveer 40%.

¹ M. C. Standage, 1973, Ph. D. Thesis, University of Otago, New Zealand.

² A. Skerbele and E. N. Lassette, *J. Chem. Phys.* 56, 845 (1972).

X

Bij hun berekening van de scrieweerstand van een keramische meerlaagscondensator bij hoge frequenties geven Coda en Selvaggi¹ niet aan onder welke voorwaarde de door hen gemaakte verwaarlozing van kringstroom-effecten is toegestaan.

¹ N. Coda and J. A. Selvaggi, *IEEE Trans. PHP* 12, 206 (1976).

XI

In de heden ten dage nog steeds voor de polijstsnelheid gebruikte formule van Archard¹ ontbreekt de afhankelijkheid van de korreldiameter van het polijstpoeder.

¹ E. Rabinowicz, 'Friction and wear of materials', Wiley, New York, 1965, Ch. 6.

XII

De door Maher¹ gebruikte formules voor de beschrijving van de defectchemie van de met zilver gedoteerde PLZT (lood/lanthaan zirkonaat/titanaat) materialen zijn niet alle correct.

¹ G. H. Maher, *J. Am. Ceram. Soc.* 66, 408 (1983).

XIII

De elektronen in een lage-druk kwik-ontlading hebben een Maxwell'se energieverdeling, in tegenstelling tot de situatie in een lage-druk edelgasontlading (Langmuir paradox)¹. Het is anno 1985 merkwaardig dat deze paradox nog niet is opgelost².

¹ I. Langmuir and H. Mott-Smith, *Gen. Electr. Rev.* 27, 616 (1924).

² V. M. Milenin and N. A. Timofeev, *Sov. Phys. Tech. Phys.* 23, 1048 (1978).

XIV

Een goede mondhygiëne is goud waard.

P. Axelsson and J. Lindhe, *J. of Clinical Periodontol.* 8, 239 (1981).
H. van Herk, *NVM-tijdschrift* 9, no.2, 19 (1985).

XV

Het meten van de stralende vervalsnelheid van een verzameling aangeslagen atomen 'at late times' hoeft niet per se 's nachts plaats te vinden. Dit laatste kan echter vooral 's zomers wel de onderzoeksnelheid bevorderen.